Journal of Medicinal Chemistry

PURDUE UNIVERSITY

Subscriber access provided by Purdue University Libraries

Article

Exploring Basic Tail Modifications of Coumarin-based Dual Acetylcholinesterase-Monoamine Oxidase B Inhibitors: Identification of Water-soluble, Brain-permeant Neuroprotective Multitarget Agents

Leonardo Pisani, Roberta Farina, Marco Catto, Rosamaria Iacobazzi, Orazio Nicolotti, Saverio Cellamare, Giuseppe Felice Mangiatordi, Nunzio Denora, Ramón Soto-Otero, Lydia Siragusa, Cosimo Damiano Altomare, and Angelo Carotti

J. Med. Chem., **Just Accepted Manuscript** • DOI: 10.1021/acs.jmedchem.6b00562 • Publication Date (Web): 27 Jun 2016

ACS Publications

Journal of Medicinal Chemistry is published by the American Chemical Society. 1155 Sixteenth Street N.W., Washington, DC 20036

Exploring Basic Tail Modifications of Coumarin-based Dual Acetylcholinesterase-Monoamine Oxidase B Inhibitors: Identification of Water-soluble, Brain-permeant Neuroprotective Multitarget Agents

Leonardo Pisani,[a] Roberta Farina,[a] Marco Catto,[a] Rosa Maria Iacobazzi,[a] Orazio Nicolotti,[a] Saverio Cellamare,[a] Giuseppe Felice Mangiatordi,[a] Nunzio Denora,[a] Ramon Soto-Otero,[b] Lydia Siragusa,[c] Cosimo Damiano Altomare,[a] Angelo Carotti[a]*

[a] Dipartimento di Farmacia - Scienze del Farmaco, Università degli Studi di Bari "Aldo Moro", via E. Orabona, 4, I-70125 Bari, Italy
[b] Departamento de Bioquimica y Biologia Molecular, Facultad de Medicina, Universidad de Santiago de Compostela, San Francisco I, E-15782, Santiago de Compostela, Spain
[c] Molecular Discovery Limited 215 Marsh Road, Pinner, Middlesex, London HA5 5NE, UK

RECEIVED DATE

KEYWORDS: monoamine oxidase inhibitors; acetylcholinesterase inhibitors; multitarget ligand design; Alzheimer's disease; neuroprotective agents; neurodegenerative diseases; coumarin derivatives.

Abstract

Aiming at modulating two key enzymatic targets for Alzheimer's disease (AD), i.e., acetylcholinesterase (AChE) and monoamine oxidase B (MAO B), a series of multitarget ligands was properly designed by linking the 3,4-dimethylcoumarin scaffold to 1,3- and 1,4-substituted piperidine

moieties, thus modulating the basicity to improve the hydrophilic/lipophilic balance. After *in vitro* enzymatic inhibition assays, multipotent inhibitors showing potencies in the nanomolar and in the low micromolar range for hMAO B and eeAChE, respectively, were prioritized and evaluated in human SH-SY5Y cell-based models for their cytotoxicity and neuroprotective effect against oxidative toxins (H_2O_2, rotenone and oligomycin-A). The present study led to the identification of a promising multitarget hit compound **(5b)** exhibiting high hMAO B inhibitory activity (IC_{50} = 30 nM) and good MAO B/A selectivity (Selectivity Index, SI = 94) along with a micromolar eeAChE inhibition (IC_{50} = 1.03 μM). Moreover, **5b** behaves as a water-soluble, brain-permeant neuroprotective agent against oxidative insults without interacting with P-gp efflux system.

Introduction

The incidence and socio-economic costs of neurodegenerative diseases (NDs) are constantly growing as a consequence of the increased life expectancy and ageing population. Among NDs, a major role is played by Alzheimer's disease (AD), representing the most common cause of dementia. As population ages, the devastating impact of AD increases worldwide, being estimated that more than 100 million individuals will suffer from AD by 2050.[1] Alzheimer's patients experience an irreversible cognitive decline, associated with severe memory, attention and learning deficits impairing daily life activities. In the last decades, massive investments in both academic and private settings, even though lower than in other healthcare programs (e.g., anticancer therapies), have been devoted to the discovery of novel diagnostic and therapeutic tools against AD. Unfortunately, the road to effectively treat AD with both small molecules and immunotherapies addressing amyloid as well as tau hypotheses[2] has been paved with failures[3] even in late-stage clinical trials,[4] and disease-modifying drugs are missing. The disheartening attrition rate has commonly been ascribed to the multifactorial etiopathogenesis of AD exhibiting several neuronal aberrations spanning from proteostasis,[5] metal unbalance,[6] oxidative stress to mitochondrial dysfunctions,[7] ultimately leading to disruption of cholinergic transmission in

hippocampus and frontal cortex.[8] It is still a matter of debate whether researchers are addressing the wrong targets and/or the disease models are not appropriate.

So far, with the exception of memantine (approved in 2003),[9] the restoration of basal neurotransmitter acetylcholine (ACh) levels through acetylcholinesterase (AChE) inhibitors (Chart 1; donepezil, galantamine and rivastigmine) is the only approved, albeit palliative, therapeutic strategy in mild forms of AD.[10] In more recent years, the research shifted to the more promising multitarget strategy,[11] rooted on the principle that a combination of actions may be beneficial for multifactorial pathologies including AD[12] by hitting two or more relevant targets with the same molecular entity.[13,14] In many anti-Alzheimer multitargeting programs, chelation of biometals,[15] agonism to 5-HT_4 receptors,[16] antagonism to 5-HT_{1A} receptors,[17] radical scavenging,[18] release of vasodilating NO radical[19,20] have been considered valuable biochemical activities that could synergistically improve the therapeutic potential of AChE inhibition often remaining the core feature of multipotent agents.

AChE (EC 3.1.1.7) is a serine hydrolase responsible for the deacetylation of ACh in both central and peripheral nervous system.[21] A 20 Å narrow tunnel, chiefly lined by aromatic residues, separates a catalytic anionic site (CAS),[22] close to the catalytic triad, from another anionic subsite (peripheral anionic site, PAS) that binds the cationic heads of gorge-spanning dual binding site (DBS) inhibitors and acts as chaperone-like motif during the formation of Aβ oligomers.[23] Another ChE isoform (butyrylcholinesterase, BChE, EC 3.1.1.8)[24] has the same biological function and its inhibitors may also have impact in the therapy of AD[25] since its activity increases in advanced AD forms.[26] To alleviate oxidative stress conditions of degenerating neurons, the inhibition of MAO (amine-oxygen oxidoreductase; EC 1.4.3.4) activity might be addressed.[27] This flavoenzyme catalyzes the degradation of endogenous and xenobiotic amines (including many neurotransmitters as catecholamines and serotonin) and contributes to increase reactive oxygen species (ROS) level through its catalytic cycle by producing the corresponding aldehyde metabolite and hydrogen peroxide as the end products. The two known isoforms, termed MAO A and MAO B,[28,29] differ in amino acid sequences, tissue distribution

and selectivity for substrates and inhibitors. As far as the role of MAO in AD is concerned, the potential application of MAO inhibitors in therapy needs to address a crucial selectivity issue. In fact, strong dietary restrictions[30] are required to avoid unwanted side effects[31] associated to the blockade of peripheral MAO A by non-selective inhibitors. Moreover, MAO B predominates in brain tissue and its activity increased in the elderly, especially in glial cells.[32]

As a part of our ongoing research on multi-functional ligands against NDs,[17,33] we recently devoted our efforts to the identification of coumarin-based AChE-MAO B inhibitors with improved drug-like properties.[34] Among privileged heterocycles, the coumarin core has been extensively decorated by several research groups addressing the discovery of novel selective MAO[35-39] and AChE[40-42] inhibitors as well as to build new molecular scaffolds with dual AChE-MAO activity[43] against NDs, in most cases through a conjugative approach.[44,45] Over the past decade, our contribution to this field highlighted the important role of substituents at position 4 and 7 of coumarin in tuning MAO B activity and selectivity.[46-50] Aiming at obtaining multipotent compounds with good overall pharmacokinetic properties, we herein focused on modifications of the basic head of the side chain at C7 and of the spacer connecting the two key pharmacophore features (namely, the basic head and the coumarin core) in order to improve aqueous solubility while maintaining a dual AChE-MAO B inhibitory activity. Starting from a potent MTDL (Multi-Target Directed Ligand),[34] the new molecular framework was built as depicted in Figure 1. The lipophilic phenyl ring was removed from the spacer and the basic nitrogen was enclosed in a flexible piperidine cycle, thus modulating the pK_a of N-sp^3 and the aqueous solubility at physiological pH. By approaching this ring-closing strategy around the basic nitrogen, we conceived a series of 2*H*-chromen-2-ones bearing a donepezil-inspired benzylpiperidine moiety that may efficiently interact with AChE binding pocket.[51] 3,4-Dimethylcoumarin was exploited as a molecular fragment to enhance MAO B affinity since this scaffold proved to be efficiently accommodated in the lipophilic enzymatic pocket that faces the FAD coenzyme and is unable to lodge sterically hindered groups.[34,52,53]

The designed compounds were tested *in vitro* to evaluate their ability to inhibit both ChEs and MAOs. The ability of novel compounds to permeate blood-brain barrier (BBB) was preliminarily calculated in silico by using Volsurf+ package (Molecular Discovery, London, UK) to compute LogBB, a Molecular Interaction Field (MIF) based parameter useful to estimate the CNS distribution of small molecules.[54] The most promising compounds fished out from both the enzymatic screening and in silico BBB-permeation prediction, were prioritized and studied in human SH-SY5Y neuroblastoma cell lines for their cytotoxicity and potential neuroprotective effects against oxidative insults (hydrogen peroxide, rotenone and oligomycin A). Moreover, compounds endowed with the highest neuroprotective effects were evaluated *in vitro* for their ability to cross BBB in a Madin-Darby Canine Kidney (MDCKII-MDR1) cell model and to interact with glycoprotein-P (P-gp) mediated transport. The hydrophilic/lipophilic balance of selected compounds was investigated through well-established turbidimetric determination of aqueous solubility and RP-HPLC lipophilicity measurements.

Chemistry

Scheme 1 illustrates the synthetic pathway to piperidine derivatives **4a-m** and (±)-**5a-i** reported in Table 1. The preparation of compounds bearing a methylene spacer started from the activation of Boc-protected 3- and 4-piperidinemethanol **1b-c** as mesylate esters (**1d-e**) that underwent SN with 3,4-dimethyl-7-hydroxycoumarin in DMF at 70 °C by using cesium carbonate as the base and triethylamine to buffer the reaction mixture, thus obtaining intermediates **2b-c.** Coumarins lacking the methylene linker were synthesized starting from the Mitsunobu etherification to couple **1a** with 3,4-dimethyl-7-hydroxycoumarin[55] under buffered conditions through triethylamine, thus yielding **2a**. The removal of the carbamate protecting group of **2a-c** in acidic conditions by TFA unmasked the piperidine intermediates **3a-c** that underwent final alkylation under microwave-assisted nucleophilic substitution conditions (compounds **4b-h**, **4j-m**, (±)-**5a-i**) in acetonitrile with the appropriate benzyl bromide or methylation at room temperature (**4a**, **4i** and (±)-**5a**). $NaBH(OAc)_3$ mediated the reductive amination of

3c and commercially available 3,4-dimethoxybenzaldehyde to prepare coumarin (±)-**5i**. A sequential two-steps alkylation protocol under microwave irradiation afforded the rigid 1,2,3,4-tetrahydroisoquinoline derivatives **7a**-**b** (Scheme 2). Initially, 3,4-dimethyl-7-hydroxycoumarin was reacted with 1,3- or 1,4-dibromoalkane, thus furnishing intermediate bromides **6a**-**b**. Under the same reaction conditions, the suitable 1,2,3,4-tetrahydroisoquinoline was alkylated with **6a**-**b** yielding the desired compounds **7a-b**.

Biological assays

All compounds were tested *in vitro* for their inhibitory activities on human MAOs (hMAOs), electric eel AChE (eeAChE) and equine serum BChE (esBChE) enzymes. For hMAOs inhibition assay the protocol was carried out with a fluorescence-based method using kynuramine as a non-selective substrate of hMAO A and hMAO B.[34,56] As for ChEs, the well-known Ellman's spectrophotometric test[57] was used to determine IC_{50}s for both isoforms. The inhibition data are reported in Table 1 as IC_{50} (μM) or, for poorly active compounds, as percentage of inhibition at 10 μM. The kinetic behavior of compound (±)-**5b** for the inhibition of eeAChE was investigated and is illustrated in Figure 2 by means of Lineweaver-Burk diagram where the reciprocals of enzyme activity (eeAChE) vs. reciprocals of substrate (S-acetylthiocholine) concentration in the presence of different concentrations (0-8 μM) of inhibitor have been reported.

Human neuroblastoma SH-SY5Y cell lines were used to evaluate the cytotoxic effect of compounds **4j**-**k**, (±)-**5a**-**e** and (±)-**5i** through the 3-(4,5-dimethylthiazol-2-yl)-2,5-diphenyltetrazolium bromide (MTT) viability assay (Figure 3).[58] By using the same cellular models,[59] the ability of selected compounds to protect neurons against three different toxic insults (hydrogen peroxide, oligomycin-A and rotenone) was studied (Figure 4) and compared to donepezil taken as a reference anti-Alzheimer's drug. Data concerning cytotoxicity and neuroprotection assays are expressed as percentage of viability referred to control experiment as illustrated in Figures 3 and 4.

As previously reported,[34] cell-based transport studies were aimed at monitoring the BBB permeating potential of compounds (±)-**5a**-**b** and (±)-**5d** displaying the highest neuroprotective activity. Bidirectional transport studies were carried out by measuring apical to basolateral (AP-BL) and basolateral to apical (BL-AP) apparent permeability (P_{app}) in MDCK cells. After retroviral transfection with the human MDR1 cDNA (MDCKII-MDR1), these cells highly express P-gp thus alerting compounds likely to be efflux pumps substrates. P_{app} (in units of cm/sec) and efflux ratio (ER) were calculated and summarized in Table 2.

Results and discussion

It is worth underlining that MAO B selectivity of the multipotent ligands reported herein was a pursued feature to avoid well-known side effects raising from the inhibition of peripheral MAO A isoform. On the other hand, isoform selectivity was not considered a crucial issue in the case of ChEs. In fact, in advanced AD increasing body of evidence supports the importance of BChE whose activity increases as the disease progresses. Both ChEs are capable of catalyzing the hydrolysis of ACh. Therefore, BChE inhibition can be a viable strategy to counteract the cholinergic depletion too.[25]

Keeping the 3,4-dimethylcoumarin as the common structural feature, the main modifications regarded the flexibility and geometry of the linker tethering the coumarin backbone at position 7 to the basic head and the alkylation of the piperidine nitrogen.

Looking at the inhibition data for piperidine-bearing coumarins reported in Table 1, as expected from the presence of the *N*-benzylpiperidine moiety mimicking donepezil, all compounds showed from good to high affinity towards AChE (IC_{50}s ≤ 10 μM) along with good selectivity values over BChE. AChE inhibitory potencies shift was not remarkably influenced by the structural modification herein reported and IC_{50}s for AChE laid in the range 0.68 μM (**4i**) – 9.57 μM (**4l**). In contrast, a wider activity window could be observed for MAO B (0.030 μM for (±)-**5b** < IC_{50}s < 2.49 μM for **4g**) suggesting a more pronounced effect of the substitution pattern on the MAO affinity.

All hybrids displayed from moderate to high affinity towards hMAO B with submicromolar IC_{50}s but for **4b** and **4g**. All compounds inhibited selectively MAO B, with Selectivity Index (SI, IC_{50} MAO A / IC_{50} MAO B) ranging from 2 (**4e**-**f**) to 133 ((±)-**5h**).

Furthermore, MAO B affinity was affected by the flexibility of the linker and the piperidine substitution site (3 vs. 4) more than AChE affinity. In fact, higher MAO B inhibitory potencies could be fished out from compounds **4i**-**m** and (±)-**5a**-**i** where a methylene spacer tethers the basic head to the planar coumarin. In absence of the spacer, increasing the size and lipophilicity of the substituent on piperidine nitrogen from methyl (**4a)** to *n*-butyl (**4b**) and benzyl group (**4c**) decreased MAO B affinity while improving AChE affinity. The opposite trend was observed in presence of the methylene linker connecting the coumarin to the 3- and 4-substituted piperidinyl ring when moving from methyl to benzyl (**4i** vs. **4j**, **(±)-5a** vs. (±)-**5b**). Homologation of the terminal chain from benzyl (**4c**) to phenethyl (**4g**) group influenced negatively the affinities towards both MAOs and reduced AChE affinity, too. The introduction of a carbonyl group (**4h**) produced a 4-fold MAO B affinity improvement with respect to **4c** whereas AChE inhibitory potency diminished.

The substitution position at the piperidine cycle strongly influenced MAO B affinity. As a matter of fact, three derivatives out of the 4-substituted piperidine series (**4a**-**m)** showed an IC_{50} < 0.250 μM whereas all 3-substituted piperidines (±)-**5a**-**i** showed MAO B inhibitory potencies < 0.250 μM. The presence of 3-substituted piperidines was preferred from MAO B with respect to 4-piperidinyl moieties ((±)-**5a** > **4a** and **4b**; (±)-**5b** > **4c** and **4j**; (±)-**5c** > **4d** and **4k**; (±)-**5f** > **4e** and **4l**; (±)-**5h** > **4f** and **4m**), irrespective of the nitrogen substituents. Looking at the basic head, the introduction of halogens (3'-Cl, 3'-Br, 4'-F, 4'-Cl) as well as electron-withdrawing (4'-SO_2CH_3 and 4'-CN) and electron-donating groups (3',4'-diOMe) on the phenyl ring exhibited a detrimental effect regards to MAO B affinity and drastically reduced MAO B/A selectivity. *Meta*-substitution represented the preferred position for chlorine in the binding to MAO B enzymatic cleft, as inferred by comparing **4d** vs. **4e**, **4k** vs. **4l**, (±)-**5c** vs. (±)-**5f**. In *para* position a cyano group was preferred to chloro (**4e** < **4f**, **4l** < **4m**, (±)-**5f** < (±)-**5h**) in

both MAO B and AChE. Sulfonyl derivative (±)-**5g** displayed the highest MAO A affinity along with a low IC_{50} towards MAO B.

To assess the AChE inhibition mechanism of donepezil-like *N*-benzyl-piperidines the kinetic behaviour of compound (±)-**5b** was investigated. As shown in Figure 2, Lineweaver-Burk plot indicated a mixed-type inhibition with a K_i equal to 1.37 ± 0.05 μM, thus suggesting a partial occupancy of PAS and potential Aβ anti-aggregating properties.

HPLC separations were undertaken to check a possible influence of chirality in the binding interactions of this series, and racemic mixtures of **5b** and **5d** were resolved as prototypes on a CHIRALPAK IA column yielding enantiomeric excess > 99% (see Supporting Information for details). Regarding hMAO B affinity, an eudismic ratio equal to 8 was observed for both racemates. Eutomers (+)-**5b** and (+)-**5d** exhibited outstanding hMAO B affinities (IC_{50} = 23 and 26 nM, respectively). Interestingly, the most potent enantiomer (+)-**5b** showed also an outstanding MAO B over MAO A selectivity (SI = 167), much greater than the other eutomer (+)-**5d** (SI = 21). Both mixtures displayed a lower activity ratio (≤ 2) towards hMAO A, being (+)-**5b** and (−)-**5d** the distomers. A lower and inverted eudismic ratio was found towards eeAChE for both pairs of enantiomers.

To overcome the undesirable drawback of chirality, 1,2,3,4-tetrahydroisoquinoline derivatives **7a-b** were designed as rigid achiral analogues of the most potent hit compound ((±)-**5b**). *In vitro* evaluation proved a sharp drop of MAO B affinity albeit the potency was still in the nanomolar range. Interestingly, compounds **7a-b** showed low micromolar affinities towards both ChEs, with **7a** being the most potent BChE inhibitor of the whole series with a submicromolar IC_{50} = 0.95 μM. This result could be ascribed to the flatness and wideness of BChE enzymatic cleft that could better accommodate rigid and sterically hindered basic groups.

To assess the brain-permeating capability of the novel multipotent molecules reported herein, Volsurf+ was employed to compute LogBB, a parameter expressing the logarithmic ratio between the concentration of a drug in brain and blood. More specifically, compounds showing logBB value greater than 0.5 readily penetrate into CNS and are classified as BBB+. LogBB values lower than -0.5 disclose

very poor brain permeation (BBB- compounds) whereas values higher than -0.5 and lower than 0.5 indicate moderate permeation (BBB± compounds).[60] Calculations suggested that most compounds in Table 1 should rapidly be distributed into the brain (BBB+ compounds). LogBB of derivatives bearing polar substituents on the phenyl ring (a cyano-group for **4f**, **4m** and (±)-**5h** or a dimethoxy-group for (±)-**5i**) and the keto-derivative **4h** suggested moderate permeation. The lowest logBB value (0.011) was returned by (±)-**5g** with a highly hydrophilic substituent on the basic head (-SO_2CH_3 group). The high confidence of Volsurf-based predictions was assessed through the projection of the studied compounds in the chemical space represented by its applicability domain, determined according to the Hotelling's T-Squared approach (see Supporting Information).[61]

Cell-based assays: cytotoxicity, neuroprotection and brain-permeation

By combining data from enzymatic screening with in silico calculations, a number of hits was shortlisted and selected for further assays in cell-based models in order to evaluate their cytotoxic and neuroprotective effects and their ability to permeate BBB without interacting with efflux pumps such as P-gp. Regarding the inhibitory properties, the following selection criteria were applied: i) IC_{50} towards MAO B < 150 nM; ii) IC_{50} towards AChE < 2 μM. With respect to brain permeation predictions, logBB threshold was set equal to 0.450. Seven coumarin derivatives (**4j**, **4k**, (±)-**5a**, (±)-**5b**, (±)-**5c**, (±)-**5d** and (±)-**5e**) met all the selection criteria and were submitted to preliminary *in vitro* investigations in human neuroblastoma SH-SY5Y cell lines. Compound (±)-**5i** was also included in the study in order to investigate the effect of the ortho-dimethoxyphenyl moiety.

Since *in vitro* enzymatic assays for both enantiomers of **5b** and **5d** provided AChE inhibition activities close to racemate and the differences between enantiomers and racemate for MAO B were reasonably low (ratio of IC_{50}s < 6 for both isomers in comparison to racemate **5b** and **5d**), we deemed unnecessary to perform the cell-based studies on single enantiomers at this early stage investigations.

As shown in Figure 3, most compounds displayed negligible cytotoxicity up to 50 μM after 24 h incubations. Some derivatives produced a reasonable cellular damage only at highest concentrations. In

particular, the concentrations responsible for 50% inhibition of cell growth (IC_{50}s) for compounds (±)-**5a**, (±)-**5b**, (±)-**5c** and (±)-**5i** were equal to 30 ± 0.01 μM, 44 ± 0.02 μM, 13 ± 0.01 μM and 10 ± 0.03 μM, respectively.

The overproduction of harmful radicals, above all reactive oxygenated species (ROS), and the unbalance in detoxification systems produces severe oxidative stress conditions in neurons affected by AD. Nucleic acids, proteins and lipids become loaded with aberrant alterations that, in turn, could trigger AD-related neurotoxicity and indeed the reduction of oxidative stress has been claimed as a viable strategy to slow down the progression of the disease. Therefore, we tested also the ability of selected multitarget molecules to protect SH-SY5Y cells against oxidative injuries. The cytoprotective effect was determined by measuring cell viability after incubation with a radical initiator (hydrogen peroxide, H_2O_2) and two mitochondrial poisons (rotenone and oligomycin-A), both capable of arresting respiratory chain and energy production (Figure 4). Rotenone induces cellular damage by interfering with the activity of complex I of the respiratory chain[62] whereas oligomycin-A binds to F_o part of H^+-ATP-synthase[63] and exerts its pro-apoptotic effect by blocking ATP formation. Compounds under investigation were incubated at two concentrations (1 and 10 μM) and untreated cells were used as control. As depicted in Figure 4a, compounds (±)-**5a-e** markedly protected SH-SY5Y cells against H_2O_2 even at the lowest concentration (1 μM). A low increase of cell viability in the presence of oligomycin-A was produced by **4j** (at 1 and 10 μM), **4k** (at 1 μM), (±)-**5c** (at 10 μM) and (±)-**5i** (at 1 and 10 μM). Moreover, derivative (±)-**5a** was not able to counteract cellular damage induced by oligomycin-A, whereas it exerted a moderate neuroprotective activity against rotenone at 1 and 10 μM. A significant increase of viable cells was obtained when rotenone was co-incubated with (±)-**5e** at 1 μM. Derivative (±)-**5b** and (±)-**5d** remarkably increased cell viability in the presence of both mitochondrial toxins used in this assay (rotenone and oligomycin-A) at 1 and 10 μM and exerted a cytoprotective activity by far superior to that of donepezil. Taken together these results highlighted dual inhibitors (±)-**5b** and (±)-**5d** as the most promising neuroprotective agents of the series, as they proved to be effective against all the insults employed in SH- SY5Y cell-based experimental models.

To endorse the potential of both compounds as promising multipotent anti AD leads, *in vitro* transport studies were undertaken. As for CNS-acting drugs, a critical issue is represented by the ability to cross BBB acting as a highly lipophilic boundary.[64] Compounds permeate BBB mainly by passive diffusion mechanism and several efflux systems prevent the entrance of xenobiotics into CNS. Since the extrusion activity is essentially governed by P-gp, the possible behavior of a hit as a P-gp substrate should be assessed in the early stage of drug discovery along with its brain permeation properties. MDCK cells were used as a model to examine the behavior of selected compounds in crossing BBB and eventually interacting with extrusion pumps. When retrovirally transfected with the human MDR1 cDNA (MDCKII-MDR1), these cell lines highly express P-gp (MDR1) and represent a robust BBB mimicking *in vitro* model. Furthermore, permeation analyses were undertaken also with (±)-**5a**, being the most potent neuroprotective agent against H_2O_2 at 10 μM and moderately effective against rotenone at both tested concentrations (1 and 10 μM). In contrast with the computed LogBB, lipophilic derivative (±)-**5d** was not able to permeate the monolayer (see Table 2), probably because of quite high membrane retention as deduced from low permeation rate in both directions, i.e., apical-to-basolateral (AP-BL) and basolateral-to-apical (BL-AP). Moreover, an ER > 2 (ER = P_{app}, BL-AP / P_{app}, AP-BL) can be taken as a figure of undesirable interactions with P-gp. On the other hand, as shown in Table 2 compounds (±)-**5b** and (±)-**5a** confirmed rapid permeation and low ER comparable to donepezil used as reference CNS-active drug, thus envisaging good brain distribution and poor interactions as P-gp substrates.

Aqueous solubility and lipophilicity

In the present work, the aim of optimizing the aqueous solubility at pH 7.4 of a coumarin-based hit recently reported by us (7-(4-(*N*-Benzyl-*N*-methylaminomethyl)benzyloxy)-4-(hydroxymethyl)-2*H*-chromen-2-one hydrochloride **I**;[34] Figure 1) while maintaining a dual AChE-MAO B inhibitory activity was pursued by introducing focused structural modification on the protonatable head and on the linker at position 7 of the coumarin core. Kinetic aqueous solubility at pH 7.4 was experimentally determined for compounds **I**, **4j**, **5a** and **5b** by applying a turbidimetric method.

As showed in Table 3, compound **I** returned the lowest value of water solubility (log S= -4.42) and the *N*-methylpiperidin-3-yl derivative **5a** exhibited the highest solubility (logS = -3.67). Compared to **I**, the piperidin-4-yl derivative **4j** showed only a modest increase of solubility (logS = -4.25), whereas the isomer piperidin-3-yl derivative **5b** proved to be 3-fold more soluble (119 μM, logS = -3.92).

The observed increase in water solubility at pH 7.4 of **4j**, **5a** and **5b** over **I**, and the small but significant differences among them as well, could be reasonably explained taking into account the pK_a shift (i.e., the degree of amine protonation) in the examined molecules and their hydrophobicity. Regarding the basicity of the amino moiety at C(7) of the coumarin core, the ACD/labs (ver. 6.00) software estimates pK_as of 7.8 for **I**, about 8.5 for **4j** and **5b**, and about 9.4 for **5a** (all values are however within the optimal range 7.5-10.5 proposed for CNS drugs).[65] The lipophilicity of the molecules in neutral form was assessed by calculation (Bio-Loom 1.6, Biobyte Corp., Claremont, U.S.A.), whereas a relative lipophilicity scale of the compounds, predominantly in the protonated form, was experimentally determined by a reversed phase (RP) HPLC method. Zorbax Eclypse-C18 column was used as the stationary phase and mixtures of ammonium acetate buffer (20 mM, pH 5.00) and methanol were used as the mobile phases to measure chromatographic capacity factor (log*k*') as a lipophilicity index.

Looking at the data in Table 3, interesting structure-property relations could be derived. Quite obviously, the most water-soluble is **5a**, that is the most hydrophilic one (i.e., the lowest log*k*' and cLogP values) and fully protonated at pH 7.4. Both *N*-benzylpiperidinyl derivatives **4j** and **5b**, despite their higher lipophilicity (as supported by the cLogP and log*k*' values), are more soluble in water than **I**, most likely due to the different protonation degree of the amino group which, based on the estimated pK_as, should be higher in **4j** and **5b** than in **I**. Albeit showing similar lipophilicity and very close basicity, the piperidin-3-yl derivative **5b** proved to be more than 2-fold more soluble in water that the isomer piperidin-4-yl compound **4j**. This result may be related on one hand to the disruption of molecular symmetry elements in **5b** with respect to **4j**, which could be an entropic factor favouring solubility in water, whereas on the other hand the proximity of the polar groups in **5b**, which are closer

than in **4j**, could explain the slightly better partitioning of **5b** in apolar media, as cLogP and log*k*' values account for.

Conclusions

The multitarget approach has been extensively exploited by several research groups as a promising therapeutic option to face neurodegenerative disorders.[66-69] In the case of AD, in the last decades inhibition of enzymatic activities of MAOs and ChEs has been pursued to identifying novel therapeutic agents with a potential disease-modifying effect.[70,71] A seminal discovery in the field is represented by ladostigil,[72] a dual AChE-MAO inhibitor,[73] that has been recently announced to finish ad interim phase IIb and to enter phase III clinical trials by Avraham Pharmaceuticals for the treatment of mild cognitive impairment.[74] Looking at the literature, common drawbacks of multitarget dual inhibitors hitting MAOs and ChEs are given by low MAO B over MAO A selectivity and, at least, one violation of Lipinski's Rule of Five (in most cases MW > 500 and/or cLogP > 5), the latter representing a compromising feature for good oral bioavailability. Peripheral inhibition of MAO A implies safety issues arising from the so-called cheese effect.[75] Over the years, we devoted attention to the development of coumarin-based dual AChE-MAO B inhibitors. To this end, our design strategy was aimed at improving the physicochemical properties for drug bioavailability (aqueous solubility, above all) of a previously described multi-potent hit compound[34] while maintaining a dual AChE-MAO B inhibitory activity. Such compound (i.e., derivative **I** in ref. 34, Figure 1) showed outstanding *in vitro* inhibitory potencies against hAChE and hMAO B in the nanomolar range along with a limited aqueous solubility at pH 7.4 (38 μM).

Structure-activity relationships (SARs) of multipotent compounds described herein shed light on the most relevant structural features modulating hMAO B affinity: i) the flexibility of the spacer linking the coumarin core to the basic tail at position 7 and ii) the substituents and the branching position on the piperidinyl ring (1,3 vs. 1,4). AChE affinity was influenced by these structural modifications to a lesser

extent. Interestingly, the presence of piperidinyl fragment along with its substitution pattern markedly influenced aqueous solubility.

The present study allowed the development of a novel multi-functional agent (±)-**5b** with a good balance of biochemical activities and improved aqueous solubility, definitively deserving further attention. *In vitro* enzymatic assays highlighted an outstanding hMAO B affinity (IC_{50} = 30 nM) along with pronounced MAO B/A selectivity (SI = 94) and low micromolar eeAChE affinity (IC_{50} = 1.03 μM). In cell-based assays, (±)-**5b** produced low cytotoxic damage (IC_{50} = 44 ± 0.02 μM) after 24 h incubation and increased cell viability of human neuroblastoma lines incubated with some toxic insults (H_2O_2, rotenone and oligomycin-A). Interestingly, its neuroprotective activity against the oxidative stress insults produced by hydrogen peroxide, oligomycin-A and rotenone was superior to that of donepezil, used as a reference anti-AD drug. Bidirectional transport studies on MDCKII-MDR1 model denoted a rapid BBB permeation without suffering from likely P-gp interactions thus suggesting good brain permeation and CNS distribution. Moreover, coumarin (±)-**5b** does not violate Lipinski's rule of five (MW = 377.48, HB-donor = 0-1 depending on the protonation state, HB-acceptor = 2-3 depending on the protonation form, cLogP (ChemAxon) = 4.57). The presence of the basic piperidinyl moiety does increase water solubility of **5b** at pH 7.4 (3-fold increase compared to **I**[34]). Taken together, these findings highlighted the potential of this class of compounds and particularly of (±)-**5b** as multitarget anti-AD neurotherapeutic, deserving further pharmacological investigations to prove its ability to prevent the onset, hamper the progression or reverse the neurodegenerative process in animal models.

Experimental section

Chemistry

Starting materials, reagents, intermediate **1a** and analytical grade solvents were purchased from Sigma-Aldrich (Europe). The purity of all the intermediates, checked by ^{1}H NMR and HPLC was always better than 95%. All the newly prepared and tested compounds showed HPLC purity higher than 98%. Column chromatography was performed using Merck silica gel 60 (0.063-0.200 mm, 70-230 mesh). Flash chromatographic separations were performed on Biotage SP1 purification system using flash cartridges prepacked with KP-Sil 32-63 μm, 60 Å silica. All reactions were routinely checked by TLC using Merck Kieselgel 60 F_{254} aluminum plates and visualized by UV light or iodine. Regarding the reaction requiring the use of dry solvents, the glassware was flame-dried and then cooled under a stream of dry argon before the use. Optical rotation was measured on a Perkin-Elmer 241 polarimeter with a Na lamp (589 nm). Nuclear magnetic resonance spectra were recorded on a Varian Mercury 300 instrument (at 300 MHz) or on a Agilent Technologies 500 apparatus (at 500 MHz) at ambient temperature in the specified deuterated solvent. Chemical shifts (δ) are quoted in parts per million (ppm) and are referenced to the residual solvent peak. The coupling constants *J* are given in Hertz (Hz). The following abbreviations were used: s (singlet), d (doublet), dd (doublet of doublet), t (triplet), q (quadruplet), qn (quintuplet), m (multiplet), br s (broad signal); signals due to OH and NH protons were located by deuterium exchange with D_2O. Chiral HPLC separations and enantiomeric excess determinations were carried out on CHIRALPAK IA (Chiral Technologies Europe, 25 cm x 0.46 cm I. D., 5 μm size particles) built on a Analytic Agilent 1260 Infinity Multidetector system equipped with 1200 Series UV-Diode Array in isocratic conditions. Elemental analyses were performed on the EuroEA 3000 analyzer only on the final compounds tested as MAOs and ChEs inhibitors. The measured values for C, H, and N agreed to within ± 0.40% of the theoretical values. Melting points were determined by the capillary method on a Stuart Scientific SMP3 electrothermal apparatus and are uncorrected.

General procedure for the synthesis of *tert*-butyl 3- and 4-hydroxymethyl piperidine-1-carboxylate (1b-c). To a suspension of the suitable commercially available 3- and 4-

hydroxymethylpiperidine (8.6 g, 75 mmol) in a mixture of acetonitrile (110 mL) and saturated aq. sodium hydrogen carbonate solution (35 mL), di-tert-butyl dicarbonate (21 g, 94 mmol) was added in portions while cooling to 0 °C. The reaction mixture was then kept to room temperature and left under magnetic stirring for 18 h. Brine (300 mL) was added and the aqueous layer was extracted with ethyl acetate (3 x 150 ml). The organic phases were collected, dried over sodium sulphate, and evaporated to dryness to give the desired product that was used without further purification.

***tert*-Butyl 4-(hydroxymethyl)piperidine-1-carboxylate (1b).** Yield: 88%. ^{1}H NMR (300 MHz, $CDCl_3$) δ: 1.06−1.19 (m, 2H), 1.44 (s, 9H), 1.60−1.74 (m, 4H), 2.69 (t, J = 12.7 Hz, 2H), 3.48 (t, J = 5.8 Hz, 2H), 4.09−4.13 (m, 2H, 1H dis. with D_2O).

***tert*-Butyl 3-(hydroxymethyl)piperidine-1-carboxylate (1c).** Yield: 94%. ^{1}H NMR (500 MHz, DMSO-d_6) δ: 1.01−1.10 (m, 1H), 1.21−1.47 (m, 3H), 1.37 (s, 9H), 1.52−1.68 (m, 2H), 2.63−2.72 (m, 1H), 3.11−3.19 (m, 1H), 3.21−3.28 (m, 1H), 3.73−3.81 (m, 1H), 3.87−3.96 (m, 1H), 4.48 (t, J = 8.8 Hz, 1H, dis. with D_2O).

General procedure for the synthesis of *tert*-butyl 4-{[(methylsulfonyl)oxy]methyl}piperidine-1-carboxylate (1d) and *tert*-butyl 3-{[(methylsulfonyl)oxy]methyl}piperidine-1-carboxylate (1e). The suitable Boc-protected piperidine **1b-c** (7.5 g, 35 mmol) was dissolved in CH_2Cl_2 (100 mL) before the addition of triethylamine (20 mL, 140 mmol). The mixture was cooled to 0 °C with an external ice bath and methanesulfonyl chloride (3.0 mL, 39 mmol) was added dropwise. After warming at room temperature, the reaction was kept under magnetic stirring for 3 h. The mixture was diluted with CH_2Cl_2 (200 mL) and washed with sat. aq. Na_2CO_3 (3 x 200 mL). The organic phase was dried over Na_2SO_4. Evaporation of the solvent yielded the desired product in high purity.

***tert*-Butyl 4-{[(methylsulfonyl)oxy]methyl}piperidine-1-carboxylate (1d).** Yield: 86%. ^{1}H NMR (500 MHz, DMSO-d_6) δ: 1.03−1.11 (m, 2H), 1.38 (s, 9H), 1.61−1.65 (m, 2H), 1.82−1.88 (m, 1H), 2.62−2.75 (br s, 2H), 3.15 (s, 3H), 3.90−3.97 (m, 2H), 4.04 (d, J = 6.4 Hz, 2H).

***tert*-Butyl 3-{[(methylsulfonyl)oxy]methyl}piperidine-1-carboxylate (1e).** Yield: 85%. ^{1}H NMR (500 MHz, DMSO-d_6) δ: 1.20−1.26 (m, 1H), 1.28−1.35 (m, 1H), 1.38 (s, 9H), 1.56−1.62 (m, 1H), 1.69−1.74 (m, 1H), 1.76−1.82 (m, 1H), 2.78−2.84 (m, 2H), 3.16 (s, 3H), 3.67−3.72 (br s, 2H), 4.01−4.10 (m, 2H).

***tert*-Butyl 4-((3,4-dimethyl-2-oxo-2*H*-chromen-7-yl)oxy)piperidine-1-carboxylate (2a).** Triethylamine (17 mL, 120 mmol), commercially available **1a** (8.1 g, 40 mmol), and 1,1'-(azodicarbonyl)-dipiperidine (20 g, 80 mmol) were added to a suspension of 3,4-dimethyl-7-hydroxycoumarin (15 g, 80 mmol) in dry CH_2Cl_2 (250 mL). The reaction mixture was kept to 0 °C and triphenylphosphine (21 g, 80 mmol), previously dissolved in CH_2Cl_2 (100 mL), was added dropwise. The reaction was kept to room temperature and left under magnetic stirring overnight. The solvent was evaporated under reduced pressure and the resulting crude solid was purified through flash chromatography (gradient eluent: ethyl acetate in *n*-hexane 20%→60%). Yield: 60%. ^{1}H NMR (300 MHz, $CDCl_3$) δ: 1.47 (s, 9H), 1.71−1.82 (m, 2H), 1.92−1.98 (m, 2H), 2.18 (s, 3H), 2.37 (s, 3H), 3.31−3.39 (m, 2H), 3.66−3.74 (m, 2H), 4.48−4.55 (m, 1H), 6.80 (d, J = 2.2 Hz, 1H), 6.84 (dd, J_1 = 2.2 Hz, J_2 = 8.8 Hz, 1H), 7.50 (d, J = 8.8 Hz, 1H).

General procedure for the synthesis of *tert*-butyl 3- or 4-(((3,4-dimethyl-2-oxo-2*H*-chromen-7-yl)oxy)methyl)piperidine-1-carboxylate (2b-c). The appropriate mesylate ester **1d-e** (8.2 g, 28 mmol) was dissolved in dry DMF (50 mL) followed by the addition of triethylamine (7.8 g, 56 mmol), cesium carbonate (9.1 g, 28 mmol) and 3,4-dimethyl-7-hydroxycoumarin (4.5 g, 28 mmol). After heating at 70 °C for 72 h, the mixture was poured onto crushed ice (500 g). The precipitate was collected and thoroughly washed with water thus furnishing the desired derivative **2b-c**.

***tert*-butyl 4-{[(3,4-dimethyl-2-oxo-2*H*-chromen-7-yl)oxy]methyl}piperidine-1-carboxylate (2b).** Yield: 85%. ^{1}H NMR (300 MHz, $CDCl_3$) δ: 1.24−1.33 (m, 2H), 1.46 (s, 9H), 1.77−1.86 (m, 2H), 1.93−2.03 (m, 1H), 2.18 (s, 3H), 2.37 (s, 3H), 2.75 (t, J = 12.4 Hz, 2H), 3.84−3.86 (m, 2H), 4.16−4.18 (m, 2H), 6.77 (d, J = 2.5 Hz, 1H), 6.83 (dd, J_1 = 2.5 Hz, J_2 = 8.8 Hz, 1H), 7.49 (d, J = 8.8 Hz, 1H).

***tert*-butyl 3-{[(3,4-dimethyl-2-oxo-2*H*-chromen-7-yl)oxy]methyl}piperidine-1-carboxylate (2c).** Yield: 89%. ^{1}H NMR (300 MHz, DMSO-d_6) δ: 1.33 (s, 9H), 1.26−1.35 (m, 2H), 1.59−1.66 (m, 1H), 1.71−1.83 (m, 1H), 1.85−1.91 (m, 1H), 2.00 (s, 3H), 2.35 (s, 3H), 2.80−2.95 (m, 2H), 3.88−3.97 (m, 4H), 6.91−6.95 (m, 2H), 7.68 (d, J = 8.8 Hz, 1H).

General procedure for the synthesis of 3,4-dimethyl-7-(piperidin-4-yloxy)-2*H*-chromen-2-one (3a) and 3,4-dimethyl-7-(piperidin-3- and 4-ylmethoxy)-2*H*-chromen-2-one (3b-c). To a solution of **2a** (7.5 g, 20 mmol) or **2b-c** (7.7 g, 20 mmol) in CH_2Cl_2 (40 mL), trifluoroacetic acid (40 mL) was added dropwise while cooling to 0 °C. After 15 minutes, the reaction mixture was kept to room temperature and left under magnetic stirring for 1 h. The solvents and excess trifluoroacetic acid were removed under reduced pressure. The resulting oil was diluted with ethyl acetate (100 mL) and washed with Na_2CO_3 (3 x 30 mL). The organic phase was dried over Na_2SO_4 and concentrated to dryness, thus obtaining the unprotected piperidines as white solids.

3,4-Dimethyl-7-(piperidin-4-yloxy)-2*H*-chromen-2-one (3a). Yield: 83%. ^{1}H NMR (500 MHz, DMSO-d_6) δ: 1.77−1.84 (m, 2H), 2.06 (s, 3H), 2.08−2.15 (m, 2H), 2.35 (s, 3H), 3.06−3.12 (m, 2H), 3.22−3.31 (m, 2H), 4.73−4.78 (m, 1H), 6.96−6.98 (m, 1H), 7.07−7.08 (m, 1H), 7.68−7.70 (m, 1H), NH not detected.

3,4-Dimethyl-7-(piperidin-4-ylmethoxy)-2*H*-chromen-2-one (3b). Yield: 89%. ^{1}H NMR (300 MHz, DMSO-d_6) δ: 1.38−1.51 (m, 2H), 1.86−1.95 (m, 2H), 2.03−2.11 (m, 5H), 2.35 (s, 3H), 2.84−2.98 (m, 2H), 3.25−3.34 (m, 2H), 3.95−3.97 (m, 2H), 6.91 (d, J = 2.5 Hz, 1H), 6.94 (dd, J_1 = 2.5 Hz, J_2 = 8.8 Hz, 1H), 7.68 (d, J = 8.8 Hz, 1H).

3,4-Dimethyl-7-(piperidin-3-ylmethoxy)-2*H*-chromen-2-one (3c). Yield: 92%. ^{1}H NMR (300 MHz, DMSO-d_6) δ: 1.21−1.38 (m, 2H), 1.58−1.64 (m, 1H), 1.80−1.84 (m, 2H), 2.05 (s, 3H), 2.19 (br s, 1H), 2.34 (s, 3H), 2.73−2.81 (m, 2H), 3.22−3.37 (m, 2H), 3.92−4.05 (m, 2H), 6.91−6.95 (m, 2H), 7.69 (d, J = 8.3 Hz, 1H).

General procedure for the synthesis of final compounds 4a, 4i and 5a. The appropriate coumarin **3a-c** (0.50 mmol) was suspended in dry acetone (5 mL) before the addition of potassium carbonate (0.069 g, 0.50 mmol) and methyl iodide (0.031 mL, 0.50 mmol). The mixture was stirred at room temperature for 6 h. The inorganic residue was then filtered off and the resulting solution was concentrated to dryness under rotary evaporation. The desired products were purified as described below.

3,4-Dimethyl-7-[(*N*-methylpiperidin-4-yl)oxy]-2*H*-chromen-2-one (4a). Purification procedure: the crude was treated with THF and the insoluble residue was filtered off. Evaporation of the solvent under rotary evaporation and crystallization from *n*-hexane furnished the desired product. Yield: 59%. Mp: 95-6 °C (*n*-hexane). ^{1}H NMR (300 MHz, $CDCl_3$) δ: 1.88−1.96 (m, 2H), 2.10−2.15 (m, 2H), 2.18 (s, 3H), 2.37 (s, 3H), 2.38 (s, 3H), 2.40−2.50 (m, 2H), 2.75−2.80 (m, 2H), 4.41 (br s, 1H), 6.80 (d, J = 2.5 Hz, 1H), 6.84 (dd, J_1 = 2.5 Hz, J_2 = 8.8 Hz, 1H), 7.49 (d, J = 8.8 Hz, 1H). Anal. ($C_{17}H_{21}NO_3$) calcd. % C, 71.06; H, 7.37; N, 4.87. Found % C, 71.39; H, 7.23; N, 5.02.

3,4-Dimethyl-7-[(*N*-methylpiperidin-4-yl)methoxy]-2*H*-chromen-2-one hydrochloride (4i). Purification procedure: the crude was treated with HCl 1.25 N in ethanol, collecting the precipitate. Yield: 65%. Mp > 250 °C. ^{1}H NMR (300 MHz, DMSO-d_6) δ: 1.57−1.65 (m, 2H), 1.91−1.96 (m, 3H), 2.05 (s, 3H), 2.35 (s, 3H), 2.68 (s, 3H), 2.89−2.99 (m, 2H), 3.36−3.42 (m, 2H), 3.94 (d, J = 6.0 Hz, 2H), 6.91−6.97 (m, 2H), 7.69 (d, J = 9.0 Hz, 1H), 10.40 (br s, 1H, dis. with D_2O). Anal. ($C_{18}H_{23}NO_3$·HCl) calcd. % C, 63.99; H, 7.16; N, 4.15. Found % C, 64.31; H, 7.26; N, 4.20.

(±)-**3,4-Dimethyl-7-[(*N*-methylpiperidin-3-yl)methoxy]-2*H*-chromen-2-one hydrochloride (5a).** Purification procedure: the crude was treated with HCl 1.25 N in ethanol yielding a precipitate that was collected and washed with ethanol. Yield: 60%. Mp: 150-2 °C. ^{1}H NMR (300 MHz, DMSO-d_6) δ: 1.19−1.30 (m, 1H), 1.70−1.89 (m, 4H), 2.06 (s, 3H), 2.35 (s, 3H), 2.76 (s, 3H), 3.25−3.54 (m, 4H), 3.89−4.08 (m, 2H), 6.91−6.97 (m, 2H), 7.70 (d, J = 9.0 Hz, 1H), 9.91 (br s, 1H, dis. with D_2O). Anal. ($C_{18}H_{23}NO_3$·HCl) calcd. % C, 63.99; H, 7.16; N, 4.15. Found % C, 63.89; H, 7.21; N, 3.93.

General procedure for the synthesis of final compounds 4b-h, 4j-m and (±)-**5b-h.** A Pyrex vessel was charged with a magnetic stirring and a Weflon bar, and then the appropriate 3,4-dimethyl-7-(piperidin-3- and 4-yloxy)-2*H*-chromen-2-one **3a-b**, or 3,4-dimethyl-7-(piperidin-3- and 4-ylmethoxy)-2*H*-chromen-2-one **3c-d** derivative (0.50 mmol) and potassium carbonate (1.0 mmol) were suspended in acetone (4.0 mL). The suitable commercially available butyl chloride (0.50 mmol, for **4b**) or substituted benzyl bromide (0.5 mmol) was added. The reactor was placed in a microwave apparatus and irradiated at 130 °C for 30 min. After cooling to room temperature, the solid residue was filtered off after thorough washing with CH_2Cl_2. The solution was concentrated to dryness, and the resulting crude was purified as detailed below. Compounds **4j-m**, (±)-**5b-h**, **7a-b** were obtained as hydrochloride salts as described later.

3,4-Dimethyl-7-[(*N*-butylpiperidin-4-yl)oxy]-2*H*-chromen-2-one (4b). Isolation procedure: column chromatography (eluent: methanol in chloroform 5%) followed by crystallization from hot ethanol. Yield: 55%. Mp: 86-7 °C (ethanol). ^{1}H NMR (300 MHz, $CDCl_3$) δ: 0.98 (t, J = 7.3 Hz, 3H), 1.39−1.46 (m, 2H), 1.91−1.98 (m, 2H), 2.18−2.23 (m, 2H), 2.20 (s, 3H), 2.38 (s, 3H), 2.76−2.83 (m, 2H), 2.93−3.04 (m, 2H), 3.06−3.12 (m, 2H), 3.42−3.46 (m, 2H), 4.76−4.79 (m, 1H), 6.81−6.85 (m, 2H), 7.54 (d, J = 8.5 Hz, 1H). Anal. ($C_{20}H_{27}NO_3$) calcd. % C, 72.92; H, 8.26; N, 4.25. Found % C, 73.34; H, 8.10; N, 3.97.

3,4-Dimethyl-7-[(*N*-benzylpiperidin-4-yl)oxy]-2*H*-chromen-2-one (4c). Isolation procedure: crystallization from hot ethanol. Yield: 82%. Mp: 111-2 °C (ethanol). ^{1}H NMR (300 MHz, $CDCl_3$) δ: 1.89−2.07 (m, 4H), 2.19 (s, 3H), 2.32−2.38 (m, 5H), 2.77−2.85 (m, 2H), 3.51−3.57 (m, 2H), 4.37−4.45 (m, 1H), 6.77-6.90 (m, 2H), 7.24−7.34 (m, 5H), 7.49 (d, J = 8.5 Hz, 1H). Anal. ($C_{23}H_{25}NO_3$) calcd. % C, 76.00; H, 6.93; N, 3.85. Found % C, 76.01; H, 6.89; N, 4.01.

3,4-Dimethyl-7-[(*N*-(3-chlorobenzyl)piperidin-4-yl)oxy]-2*H*-chromen-2-one (4d). Isolation procedure: crystallization from hot ethanol. Yield: 84%. Mp: 106-7 °C (ethanol). ^{1}H NMR (300 MHz, $CDCl_3$) δ: 1.83−1.91 (m, 2H), 2.02−2.07 (m, 2H), 2.18 (s, 3H), 2.34−2.40 (m, 5H), 2.70−2.77 (m, 2H),

3.51−3.56 (m, 2H), 4.37−4.43 (m, 1H), 6.80 (d, J = 2.5 Hz, 1H), 6.83 (dd, J_1 = 2.5 Hz, J_2 = 8.5 Hz, 1H), 7.23−7.29 (m, 3H), 7.37 (s, 1H), 7.49 (d, J = 8.5 Hz, 1H). Anal. ($C_{23}H_{24}ClNO_3$) calcd. % C, 69.43; H, 6.08; N, 3.52. Found % C, 69.70; H, 6.06; N, 3.56.

3,4-Dimethyl-7-[(*N*-(4-chlorobenzyl)piperidin-4-yl)oxy]-2*H*-chromen-2-one (4e). Isolation procedure: crystallization from hot ethanol. Yield: 87%. Mp: 140-1 °C (ethanol). ^{1}H NMR (300 MHz, $CDCl_3$) δ: 1.83−1.89 (m, 2H), 1.98−2.05 (m, 2H), 2.18 (s, 3H), 2.27−2.33 (m, 2H), 2.36 (s, 3H), 2.70−2.77 (m, 2H), 3.52 (s, 2H), 4.36−4.41 (m, 1H), 6.79 (d, J = 2.5 Hz, 1H), 6.83 (dd, J_1 = 2.5 Hz, J_2 = 8.5 Hz, 1H), 7.28−7.33 (m, 4H), 7.48 (d, J = 8.5 Hz, 1H). Anal. ($C_{23}H_{24}ClNO_3$) calcd. % C, 69.43; H, 6.08; N, 3.52. Found % C, 69.43; H, 6.13; N, 3.85.

4-[(4-((3,4-Dimethyl-2*H*-2-oxochromen-7-yl)oxy)piperidin-1-yl)methyl]benzonitrile (4f). Isolation procedure: crystallization from hot ethanol. Yield: 71%. Mp: 120-1 °C (ethanol). ^{1}H NMR (300 MHz, $CDCl_3$) δ: 1.79−2.00 (m, 4H), 2.18 (s, 3H), 2.35−2.38 (m, 5H), 2.78−2.82 (m, 2H), 3.50−3.56 (m, 2H), 4.41 (s, 1H), 6.79 (d, J = 2.5 Hz, 1H), 6.82 (dd, J_1 = 2.5 Hz, J_2 = 8.8 Hz, 1H), 7.15−7.33 (m, 4H), 7.49 (d, J = 8.8 Hz, 1H). Anal. ($C_{24}H_{24}N_2O_3$) calcd. % C, 74.21; H, 6.23; N, 7.21. Found % C, 74.74; H, 6.19; N, 7.21.

3,4-Dimethyl-7-[(*N*-(2-phenylethyl)piperidin-4-yl)oxy]-2*H*-chromen-2-one (4g). Isolation procedure: crystallization from hot ethanol. Yield: 87%. Mp: 107-8 °C (ethanol). ^{1}H NMR (300 MHz, $CDCl_3$) δ: 1.93−2.01 (m, 2H), 2.17−2.20 (m, 4H), 2.35−2.39 (m, 4H), 2.72−2.95 (m, 8H), 4.45−4.51 (m, 1H), 6.81 (d, J = 2.5 Hz, 1H), 6.84 (dd, J_1 = 2.5 Hz, J_2 = 8.5 Hz, 1H), 7.22−7.33 (m, 5H), 7.50 (d, J = 8.5 Hz, 1H). Anal. ($C_{24}H_{27}NO_3$) calcd. % C, 76.36; H, 7.21; N, 3.71. Found % C, 76.53; H, 7.14; N, 3.97.

3,4-Dimethyl-7-[(*N*-(2-phenyl-2-oxoethyl)piperidin-4-yl)oxy]-2*H*-chromen-2-one (4h). Isolation procedure: crystallization from hot ethanol. Yield: 90%. Mp: 94-6 °C (dec.) from ethanol. ^{1}H NMR (300 MHz, $CDCl_3$) δ: 1.63−1.72 (m, 2H), 2.05−2.16 (m, 2H), 2.19 (s, 3H), 2.34−2.41 (m, 5H), 2.96−3.02 (m, 2H), 4.19−4.27 (m, 2H), 4.57−4.63 (m, 1H), 6.85 (d, J = 2.5 Hz, 1H), 6.89 (dd, J_1 = 2.5 Hz, J_2 = 8.8 Hz,

1H), 7.51 (t, J = 7.1 Hz, 2H), 7.52 (d, J = 8.8 Hz, 1H), 7.64 (t, J = 7.1 Hz, 1H), 7.98 (d, J = 7.1 Hz, 2H). Anal. ($C_{24}H_{25}NO_4$) calcd. % C, 73.64; H, 6.44; N, 3.58. Found % C, 74.15; H, 6.38; N, 3.85.

3,4-Dimethyl-7-[(*N*-benzylpiperidin-4-yl)methoxy]-2*H*-chromen-2-one hydrochloride (4j). Isolation procedure: column chromatography (eluent: ethyl acetate in chloroform 50%). The compound was transformed into the corresponding hydrochloride salt by dissolving the solid free base in the minimum volume of 1,4-dioxane before adding HCl 4.0 N in 1,4-dioxane. The resulting precipitate was collected by filtration and washed with dry dioxane, yielding **4j**. Yield: 60%. Mp: 215-6 °C (dec.). ^{1}H NMR (300 MHz, DMSO-d_6) δ: 1.87−1.95 (m, 2H), 2.06 (s, 3H), 2.22−2.29 (m, 3H), 2.35 (s, 3H), 2.79−2.84 (m, 2H), 3.13−3.20 (m, 2H), 3.91−4.03 (m, 2H), 4.31−4.35 (m, 2H), 6.88−6.96 (m, 2H), 7.46−7.58 (m, 5H), 7.69 (d, J = 9.1 Hz, 1H), 9.68 (s, 1H, dis. with D_2O). Anal. ($C_{24}H_{27}NO_3$·HCl) calcd. % C, 69.64; H, 6.82; N, 3.38. Found % C, 70.09; H, 6.55; N, 3.40.

3,4-Dimethyl-7-[(*N*-(3-chlorobenzyl)piperidin-4-yl)methoxy]-2*H*-chromen-2-one hydrochloride (4k). Isolation procedure: the crude was suspended in 1,4-dioxane and the insoluble residue discarded. HCl 4.0 N in 1,4-dioxane was added to the solution, yielding a white precipitate that was filtered and crystallized from hot ethanol. Yield: 99%. Mp: 246-8 °C (ethanol). ^{1}H NMR (300 MHz, DMSO-d6) δ: 1.55−1.66 (m, 2H), 1.90−1.97 (m, 3H), 2.06 (s, 3H), 2.35 (s, 3H), 2.89−3.00 (m, 2H), 3.35−3.42 (m, 2H), 3.94 (d, J = 6.0 Hz, 2H), 4.26−4.30 (m, 2H), 6.91 (dd, J_1 = 2.5 Hz, J_2 = 8.8 Hz, 1H), 6.95 (d, J = 2.5 Hz, 1H), 7.48−7.55 (m, 3H), 7.66−7.71 (m, 2H), 10.16 (s, 1H, dis. with D_2O). Anal. ($C_{24}H_{26}ClNO_3$·HCl) calcd. % C, 64.29; H, 6.07; N, 3.12. Found % C, 64.68; H, 5.88; N, 2.83.

3,4-Dimethyl-7-[(*N*-(4-chlorobenzyl)piperidin-4-yl)methoxy]-2*H*-chromen-2-one hydrochloride (4l). Isolation procedure: the crude was suspended in 1,4-dioxane and the insoluble residue was discarded after filtration. HCl 4.0 N in 1,4-dioxane was added to the solution, yielding a white precipitate that was filtered and crystallized from hot ethanol. Yield: 77%. Mp > 250 °C (ethanol). ^{1}H NMR (300 MHz, DMSO-d_6) δ: 1.57−1.65 (m, 2H), 1.92−1.97 (m, 3H), 2.05 (s, 3H), 2.35 (s, 3H), 2.91−2.99 (m, 2H), 3.38−3.45 (m, 2H), 3.94 (d, J = 6.0 Hz, 2H), 4.25−4.28 (m, 2H), 6.91 (dd, J_1 = 2.5 Hz, J_2 = 8.5 Hz, 1H), 6.95 (d, J = 2.5 Hz, 1H), 7.53 (d, J = 8.8 Hz, 2H), 7.58 (d, J = 8.8 Hz, 2H), 7.67

(d, *J* = 8.5 Hz, 1H), 10.12 (s, 1H, dis. with D_2O). Anal. ($C_{24}H_{26}ClNO_3 \cdot HCl$) calcd. % C, 64.29; H, 6.07; N, 3.12. Found % C, 64.70; H, 6.00; N, 3.05.

4-[(4-((3,4-Dimethyl-2*H*-2-oxochromen-7-yl)oxymethyl)piperidin-1-yl)methyl]benzonitrile hydrochloride (4m). Isolation procedure: the crude was suspended in 1,4-dioxane and the insoluble residue was filtered off. HCl 4.0 N in 1,4-dioxane was added to the solution, yielding a white precipitate that was filtered and crystallized from hot ethanol. Yield: 93%. Mp > 250 °C (ethanol). ^{1}H NMR (300 MHz, DMSO-d_6) δ: 1.64−1.79 (m, 2H), 1.88−1.97 (m, 3H), 2.05 (s, 3H), 2.34 (s, 3H), 2.94 (q, *J* = 12.0 Hz, 2H), 3.36−3.43 (m, 2H), 3.93 (d, *J* = 6.3 Hz, 2H), 4.32−4.37 (m, 2H), 6.90−6.99 (m, 2H), 7.68 (d, *J* = 8.5 Hz, 1H), 7.86 (d, *J* = 8.4 Hz, 2H), 7.94 (d, *J* = 8.4 Hz, 2H), 11.17 (s, 1H, dis. with D_2O). Anal. ($C_{25}H_{26}N_2O_3 \cdot HCl$) calcd. % C, 68.41; H, 6.20; N, 6.38. Found % C, 68.86; H, 6.03; N, 6.17.

(±)-**3,4-Dimethyl-7-[(*N*-benzylpiperidin-3-yl)methoxy]-2*H*-chromen-2-one hydrochloride (5b).** Isolation procedure: column chromatography (eluent: ethyl acetate in chloroform 50%). The compound was transformed into the corresponding hydrochloride salt by dissolving the solid free base in the minimum volume of 1,4-dioxane before adding HCl 4.0 N in 1,4-dioxane. The resulting precipitate was collected by filtration and washed with dry dioxane, yielding **5b**. Yield: 62%. Mp: 215-6 °C (dec.). ^{1}H NMR (300 MHz, DMSO-d_6) δ: 1.20−1.34 (m, 1H), 1.60−1.75 (m, 1H), 1.77−1.90 (m, 2H), 2.06 (s, 3H), 2.20−2.27 (m, 1H), 2.35 (s, 3H), 2.72−2.86 (m, 2H), 3.30−3.49 (m, 2H), 3.90−4.07 (m, 2H), 4.28−4.33 (m, 2H), 6.90 (dd, J_1 = 2.5 Hz, J_2 = 8.8 Hz, 1H), 6.93 (d, *J* = 2.5 Hz, 1H), 7.42−7.57 (m, 5H), 7.69 (d, *J* = 8.8 Hz, 1H), 10.12 (br s, 1H, dis. with D_2O). Anal. ($C_{24}H_{27}NO_3 \cdot HCl$) calcd. % C, 69.64; H, 6.82; N, 3.38. Found % C, 69.90; H, 6.81; N, 3.56.

(+)-**3,4-Dimethyl-7-[(*N*-benzylpiperidin-3-yl)methoxy]-2*H*-chromen-2-one (5b).** HPLC purification of (±)-**5b** on a CHIRALPAK IA, mobile phase: A = methanol, B = acetonitrile; isocratic elution: 20% B; flow rate = 1 mL/min; λ = 320 nm; 100 µL injection; k_2. Mp: 117-9 °C. ^{1}H NMR (500 MHz, DMSO-d_6) δ: 1.09−1.15 (m, 1H), 1.43−1.51 (m, 1H), 1.61−1.66 (m, 1H), 1.71−1.75 (m, 1H), 1.86−2.02 (m, 3H), 2.05 (s, 3H), 2.34 (s, 3H), 2.62−2.67 (m, 1H), 2.81−2.85 (m, 1H), 3.41 (d, *J* = 13.7 Hz, 1H), 3.47 (d, *J* = 13.7 Hz, 1H), 3.92 (d, *J* = 6.4 Hz, 2H), 6.87−6.90 (m, 2H), 7.19−7.23 (m, 1H),

7.25−7.30 (m, 4H), 7.65 (d, J = 8.8 Hz, 1H). $[\alpha]^{20}_{D}$ = +18.5° (c 0.13, MeOH). Anal. ($C_{24}H_{27}NO_3$) calcd. % C, 76.36; H, 7.21; N, 3.71. Found % C, 76.50; H, 7.05; N, 3.46.

(−)-**3,4-Dimethyl-7-[(*N*-benzylpiperidin-3-yl)methoxy]-2*H*-chromen-2-one (5b).** HPLC purification of (±)-**5b** on a CHIRALPAK IA, mobile phase: A = methanol, B = acetonitrile; isocratic elution: 20% B; flow rate = 1 mL/min; λ = 320 nm; 100 μL injection; k_1. Mp: 117-9 °C. ^{1}H NMR (500 MHz, DMSO-d_6) δ: 1.07−1.14 (m, 1H), 1.42−1.51 (m, 1H), 1.61−1.66 (m, 1H), 1.70−1.78 (m, 1H), 1.84−2.02 (m, 3H), 2.05 (s, 3H), 2.34 (s, 3H), 2.62−2.67 (m, 1H), 2.81−2.85 (m, 1H), 3.42 (d, J = 13.7 Hz, 1H), 3.47 (d, J = 13.7 Hz, 1H), 3.91 (d, J = 6.4 Hz, 2H), 6.87−6.90 (m, 2H), 7.18−7.23 (m, 1H), 7.26−7.30 (m, 4H), 7.64 (d, J = 8.8 Hz, 1H). $[\alpha]^{20}_{D}$ = −18.5° (c 0.13, MeOH). Anal. ($C_{24}H_{27}NO_3$) calcd. % C, 76.36; H, 7.21; N, 3.71. Found % C, 76.80; H, 6.91; N, 3.55.

(±)-**3,4-Dimethyl-7-[(*N*-(3-chlorobenzyl)piperidin-3-yl)methoxy]-2*H*-chromen-2-one hydrochloride (5c).** Isolation procedure: the crude was suspended in 1,4-dioxane and the insoluble residue was filtered off. HCl 4.0 N in 1,4-dioxane was added to the solution, yielding a white precipitate that was filtered and crystallized from hot ethanol. Yield: 98%. MP 246-8 °C (dec.) from ethanol. ^{1}H NMR (300 MHz, DMSO-d_6) δ: 1.21−1.35 (m, 1H), 1.77−1.85 (m, 3H), 2.05 (s, 3H), 2.34 (s, 3H), 2.36−2.43 (m, 1H), 2.81 (qn, J = 11.5 Hz, 2H), 3.37−3.48 (m, 2H), 3.94−4.06 (m, 2H), 4.32 (br s, 2H), 6.85−6.93 (m, 2H), 7.45−7.54 (m, 3H), 7.45−7.70 (m, 2H), 10.30 (br s, 1H, dis. with D_2O). Anal. ($C_{24}H_{26}ClNO_3 \cdot HCl$) calcd. % C, 64.29; H, 6.07; N, 3.12. Found % C, 63.82; H, 5.85; N, 2.93.

(±)-**7-{[1-(3-Bromobenzyl)piperidin-3-yl]methoxy}-3,4-dimethyl-2*H*-chromen-2-one hydrochloride (5d).** Isolation procedure: flash chromatography (gradient eluent: ethyl acetate in *n*-hexane 20%→80%). The compound was transformed into the corresponding hydrochloride salt by dissolving the solid free base in the minimum volume of 1,4-dioxane before adding HCl 4.0 N in 1,4-dioxane. The resulting precipitate was collected by filtration and washed with dry dioxane, yielding racemic **5d**. Yield: 87%. Mp: 231-2 °C. ^{1}H NMR (free base, 300 MHz, DMSO-d_6) δ: 1.05−1.18 (m, 1H), 1.46−1.53 (m, 1H), 1.62−1.75 (m, 2H), 1.89−1.97 (m, 3H), 2.05 (s, 3H), 2.34 (s, 3H), 2.61-2.65 (m, 1H), 2.79−2.82 (m, 1H), 3.39−3.51 (m, 2H), 3.94 (d, J = 6.1 Hz, 2H), 6.86−6.89 (m, 2H), 7.21−7.29

(m, 2H), 7.40−7.45 (m, 2H), 7.65 (d, J = 9.6 Hz, 1H). Anal. ($C_{24}H_{26}BrNO_3$·HCl) calcd. % C, 58.49; H, 5.52; N, 2.84. Found % C, 58.14; H, 5.48; N, 2.98.

(+)-**7-{[1-(3-Bromobenzyl)piperidin-3-yl]methoxy}-3,4-dimethyl-2*H*-chromen-2-one (5d).** HPLC purification of (±)-**5d** on a CHIRALPAK IA, mobile phase: A = methanol, B = acetonitrile; isocratic elution: 30% B; flow rate = 1 mL/min; λ = 320 nm; 100 µL injection; k_2. Mp: 119-120 °C. ^{1}H NMR (300 MHz, DMSO-d_6) δ: 1.03−1.18 (m, 1H), 1.46−1.53 (m, 1H), 1.64−1.75 (m, 2H), 1.87−1.97 (m, 3H), 2.05 (s, 3H), 2.34 (s, 3H), 2.60−2.65 (m, 1H), 2.79−2.82 (m, 1H), 3.39−3.51 (m, 2H), 3.93 (d, J = 6.1 Hz, 2H), 6.86−6.89 (m, 2H), 7.22−7.29 (m, 2H), 7.40−7.45 (m, 2H), 7.65 (d, J = 9.6 Hz, 1H). $[\alpha]^{20}_D$ = +33.5° (c 0.08, MeOH). Anal. ($C_{24}H_{26}BrNO_3$) calcd. % C, 63.16; H, 5.74; N, 3.07. Found % C, 63.50; H, 5.58; N, 3.00.

(−)-7-{[1-(3-Bromobenzyl)piperidin-3-yl]methoxy}-3,4-dimethyl-2*H*-chromen-2-one (5d). HPLC purification of (±)-**5d** on a CHIRALPAK IA, mobile phase: A = methanol, B = acetonitrile; isocratic elution: 30% B; flow rate = 1 mL/min; λ = 320 nm; 100 µL injection; k_1. Mp: 119-120 °C. ^{1}H NMR (300 MHz, DMSO-d_6) δ: 1.05−1.18 (m, 1H), 1.46−1.53 (m, 1H), 1.62−1.75 (m, 2H), 1.89−1.97 (m, 3H), 2.07 (s, 3H), 2.33 (s, 3H), 2.61−2.67 (m, 1H), 2.80−2.84 (m, 1H), 3.36−3.51 (m, 2H), 3.94 (d, J = 6.1 Hz, 2H), 6.86−6.89 (m, 2H), 7.21−7.29 (m, 2H), 7.44−7.49 (m, 2H), 7.64 (d, J = 9.6 Hz, 1H). $[\alpha]^{20}_D$ = −33.5° (c 0.08, MeOH). Anal. ($C_{24}H_{26}BrNO_3$) calcd. % C, 63.16; H, 5.74; N, 3.07. Found % C, 63.49; H, 5.36; N, 2.96.

(±)-3,4-Dimethyl-7-[(*N*-(4-fluorobenzyl)piperidin-3-yl)methoxy]-2*H*-chromen-2-one hydrochloride (5e). Isolation procedure: the crude was suspended in 1,4-dioxane and the insoluble residue was filtered off. HCl 4.0 N in 1,4-dioxane was added to the solution, yielding a white precipitate that was filtered and crystallized from hot ethanol. Yield: 98%. Mp: 228-230 °C (dec.). ^{1}H NMR (300 MHz, DMSO-d_6) δ: 1.18−1.33 (m, 1H), 1.77−1.88 (m, 3H), 2.05 (s, 3H), 2.34 (s, 3H), 2.36−2.41 (m, 1H), 2.78 (qn, J = 9.9 Hz, 2H), 3.40−3.46 (m, 2H), 3.90−4.05 (m, 2H), 4.27−4.32 (m, 2H), 6.89 (dd, J_1 = 8.8 Hz, J_2 = 2.5 Hz, 1H), 6.93 (d, J = 2.5 Hz, 1H), 7.26−7.32 (m, 2H), 7.59−7.64 (m, 2H), 7.68 (d, J =

8.8 Hz, 1H), 10.34 (br s, 1H, dis. with D_2O). Anal. ($C_{24}H_{26}FNO_3 \cdot HCl$) calcd. % C, 66.74; H, 6.30; N, 3.24. Found % C, 66.34; H, 6.22; N, 3.17.

(±)-**3,4-Dimethyl-7-[(*N*-(4-chlorobenzyl)piperidin-3-yl)methoxy]-2*H*-chromen-2-one hydrochloride (5f).** Isolation procedure: the crude was suspended in 1,4-dioxane and the insoluble residue was filtered off. HCl 4.0 N in 1,4-dioxane was added to the solution, yielding a white precipitate that was filtered and crystallized from hot ethanol. Yield: 91%. Mp: 219-221 °C (dec.) from ethanol. ^{1}H NMR (300 MHz, DMSO-d_6) δ: 1.18−1.34 (m, 1H), 1.76−1.88 (m, 3H), 2.05 (s, 3H), 2.35 (s, 3H), 2.36−2.41 (m, 1H), 2.71−2.86 (m, 2H), 3.39−3.46 (m, 2H), 3.90−4.05 (m, 2H), 4.29−4.31 (m, 2H), 6.88 (d, J = 2.5 Hz, 1H), 6.93 (dd, J_1 = 2.5 Hz, J_2 = 8.8 Hz, 1H), 7.53 (d, J = 8.5 Hz, 2H), 7.59 (d, J = 8.5 Hz, 2H), 7.68 (d, J = 8.8 Hz, 1H), 10.37 (br s, 1H, dis. with D_2O). Anal. ($C_{24}H_{26}ClNO_3 \cdot HCl$) calcd. % C, 64.29; H, 6.07; N, 3.12. Found % C, 63.86; H, 5.97; N, 3.09.

(±)-**3,4-Dimethyl-7-[(*N*-(4-(methylsulfonyl)benzyl)piperidin-3-yl)methoxy]-2*H*-chromen-2-one hydrochloride (5g).** Isolation procedure: the crude was suspended in 1,4-dioxane and the insoluble residue was filtered off. HCl 4.0 N in 1,4-dioxane was added to the solution, yielding a white precipitate that was filtered and crystallized from hot ethanol. Yield: 99%. Mp: 172-4 °C (ethanol). ^{1}H NMR (300 MHz, DMSO-d_6) δ: 1.20−1.36 (m, 1H), 1.80−1.87 (m, 3H), 2.05 (s, 3H), 2.34 (s, 3H), 2.40−2.46 (m, 1H), 2.76−2.87 (m, 2H), 3.24 (s, 3H), 3.28−3.48 (m, 2H), 3.91−4.03 (m, 2H), 4.40−4.45 (m, 2H), 6.89 (dd, J_1 = 2.5 Hz, J_2 = 8.8 Hz, 1H), 6.93 (d, J = 2.5 Hz, 1H), 7.68 (d, J = 8.8 Hz, 1H), 7.89 (d, J = 8.7 Hz, 2H), 8.00 (d, J = 8.7 Hz, 2H), 10.91 (br s, 1H, dis. with D_2O). Anal. ($C_{25}H_{29}NO_5S \cdot HCl$) calcd. % C, 61.03; H, 6.15; N, 2.85. Found % C, 60.65; H, 5.84; N, 2.91.

(±)-**4-[(3-((3,4-Dimethyl-2*H*-2-oxochromen-7-yl)oxymethyl)piperidin-1-yl)methyl]benzonitrile hydrochloride (5h).** Isolation procedure: the crude was suspended in 1,4-dioxane and the insoluble residue was filtered off. HCl 4.0 N in 1,4-dioxane was added to the solution, yielding a white precipitate that was filtered and crystallized from hot ethanol. Yield: 76%. Mp: 220-2 °C (ethanol). ^{1}H NMR (300 MHz, DMSO-d_6) δ: 1.26−1.30 (m, 1H), 1.80−1.85 (m, 3H), 2.06 (s, 3H), 2.35 (s, 3H), 2.39−2.43 (m, 1H), 2.76−2.87 (m, 2H), 3.30−3.31 (m, 1H), 3.44−3.48 (m, 1H), 3.91−4.05 (m, 2H), 4.37−4.44 (m, 2H),

6.88−6.94 (m, 2H), 7.69 (d, *J* = 8.7 Hz, 1H), 7.77 (d, *J* = 7.8 Hz, 2H), 7.95 (d, *J* = 7.8 Hz, 2H), 10.30 (br s, 1H, dis. with D_2O). Anal. ($C_{25}H_{26}N_2O_3 \cdot HCl$) calcd. % C, 68.41; H, 6.20; N, 6.38. Found % C, 68.77; H, 6.05; N, 6.17.

(±)-7-((1-(3,4-Dimethoxybenzyl)piperidin-3-yl)methoxy)-3,4-dimethyl-2*H*-chromen-2-one (5i). 3,4-Dimethyl-7-(piperidin-3-ylmethoxy)-2*H*-chromen-2-one (0.12 g, 0.40 mmol) was dissolved under magnetic stirring with 1.3 mL of 1,2-dichloroethane in a flame-dried round-bottomed flask. 3,4-dimethoxybenzaldehyde (0.66 g, 0.40 mmol) and sodium triacetoxyborohydride (0.12 g, 0.56 mmol) were added and the reaction mixture was left under magnetic stirring, at room temperature and under nitrogen atmosphere overnight. After the removal of the solvent, the solid crude was purified through flash chromatography (gradient eluent: methanol in CH_2Cl_2 0%→10%). Yield: 45%. Mp: 62-4 °C (dec.). ^{1}H NMR (300 MHz, DMSO-d_6) δ: 1.16−1.18 (m, 1H), 1.42−1.51 (m, 1H), 1.59−1.64 (m, 1H), 1.69−1.77 (m, 1H), 1.83−1.99 (m, 3H), 2.05 (s, 3H), 2.34 (s, 3H), 2.60−2.67 (m, 1H), 2.77−2.83 (m, 1H), 3.31 (d, *J* = 13.5 Hz, 1H), 3.40 (d, *J* = 13.5 Hz, 1H), 3.67 (s, 3H), 3.70 (s, 3H), 3.92−3.94 (m, 2H), 6.74−6.77 (m, 1H), 6.82−6.84 (m, 2H), 6.86−6.90 (m, 2H), 7.65 (d, *J* = 8.5 Hz, 1H). Anal. ($C_{26}H_{31}NO_5$) calcd. % C, 71.37; H, 7.14; N, 3.20. Found % C, 71.56; H, 7.10; N, 3.09.

General procedure for the synthesis of 7-(4- and 3-bromoalkyloxy)-3,4-dimethyl-2H-chromen-2-one 6a-b. A Pyrex vessel was charged with a magnetic stirring and Weflon bar and then 7-hydroxy-3,4-dimethyl-2*H*-chromen-2-one (0.57 g, 3.0 mmol) and anhydrous potassium carbonate (0.83 g, 6.0 mmol) were suspended in acetone (10 mL). The suitable commercially available dibromoalkyl derivative (15 mmol) was added. The reactor was placed in a microwave apparatus and irradiated at 130 °C for 30 min. After cooling to room temperature, the solid residue was filtered and washed with CH_2Cl_2. The solution was concentrated to dryness, and the resulting crude was purified through flash chromatography (gradient eluent as indicated below).

7-(3-Bromopropoxy)-3,4-dimethyl-2*H*-chromen-2-one (6a). Purified by flash chromatography (gradient eluent: ethyl acetate in *n*-hexane 0%→60%). Yield: 79%. ^{1}H NMR (500 MHz, DMSO-d_6) δ:

2.07 (s, 3H), 2.27 (q, J = 6.4 Hz, 2H), 2.36 (s, 3H), 3.67 (t, J = 6.4 Hz, 2H), 4.18 (t, J = 6.4 Hz, 2H), 6.95−6.98 (m, 2H), 7.70 (d, J = 8.8 Hz, 1H).

7-(4-Bromobutoxy)-3,4-dimethyl-2*H*-chromen-2-one (6b). Purified by flash chromatography (gradient eluent: ethyl acetate in *n*-hexane 0%→50%). Yield: 88%. ^{1}H NMR (500 MHz, DMSO-d_6) δ: 1.85 (qn, J = 6.4 Hz, 2H), 1.97 (qn, J = 6.4 Hz, 2H), 2.07 (s, 3H), 2.36 (s, 3H), 3.61 (t, J = 6.4 Hz, 2H), 4.10 (t, J = 6.4 Hz, 2H), 6.92−6.95 (m, 2H), 7.68 (d, J = 8.8 Hz, 1H).

General procedure for the synthesis of final compounds 7a-b. Appropriate bromide derivative **6a-b** (0.50 mmol) was suspended under magnetic stirring in acetone (4 mL) in a Pyrex microwave reactor in the presence of anhydrous potassium carbonate (0.21 g, 1.5 mmol) and catalytic amount of potassium iodide. 1,2,3,4-Tetrahydroisoquinoline (0.080 g, 0.60 mmol) was added and the vessel was placed in a microwave apparatus and heated at 130 °C for 45 min. After cooling to room temperature, the solid residue was filtered off after washing with CH_2Cl_2. The solution was concentrated to dryness, and the resulting crude was purified through flash chromatography (gradient eluent: ethyl acetate in *n*-hexane 20%→80%). The resulting solids were transformed into the corresponding hydrochlorides by dissolving the base in the minimum amount of 1,4-dioxane followed by the addition of HCl 4.0 N in 1,4-dioxane. The precipitate was collected after filtration and washed with dry 1,4-dioxane under an Ar atmosphere.

7-[3-(3,4-Dihydroisoquinolin-2(1*H*)-yl)propoxy]-3,4-dimethyl-2*H*-chromen-2-one hydrochloride (7a). Yield: 74%. Mp > 250 °C. ^{1}H NMR (free base, 300 MHz, DMSO-d_6) δ: 1.98 (qn, J = 6.4 Hz, 2H), 2.05 (s, 3H), 2.34 (s, 3H), 2.59 (t, J = 6.4 Hz, 2H), 2.65 (t, J = 5.8 Hz, 2H), 2.79 (t, J = 5.8 Hz, 2H), 3.55 (s, 2H), 4.13 (t, J = 6.4 Hz, 2H), 6.91−6.94 (m, 2H), 7.01−7.09 (m, 4H), 7.66 (d, J = 9.9 Hz, 1H). Anal. ($C_{23}H_{25}NO_3 \cdot HCl$) calcd. % C, 69.08; H, 6.55; N, 3.50. Found % C, 69.45; H, 6.58; N, 3.75.

7-[4-(3,4-Dihydroisoquinolin-2(1*H*)-yl)butoxy]-3,4-dimethyl-2*H*-chromen-2-one hydrochloride (7b). Yield: 72%. Mp: 206-8 °C. ^{1}H NMR (free base, 500 MHz, DMSO-d_6) δ: 1.67 (qn, J = 6.9 Hz, 2H), 1.79 (qn, J = 6.9 Hz, 2H), 2.07 (s, 3H), 2.36 (s, 3H), 2.46−2.48 (m, 2H), 2.64 (t, J = 5.4 Hz, 2H), 2.79 (t,

J = 5.4 Hz, 2H), 3.53 (s, 2H), 4.10 (t, J = 6.9 Hz, 2H), 6.92−6.96 (m, 2H), 7.01−7.08 (m, 4H), 7.67 (d, J = 9.8 Hz, 1H). Anal. ($C_{24}H_{27}NO_3 \cdot HCl$) calcd. % C, 69.64; H, 6.82; N, 3.38. Found % C, 69.62; H, 6.79; N, 3.63.

HPLC chiral resolution

HPLC chiral resolution of racemic **5b** and **5d** were performed on a Analytic Agilent 1260 Infinity Multidetector system equipped with 1200 Series UV-Diode Array detector using one of the following methods in a semi-preparative polar mode at room temperature. UV spectra were recorded at 230, 254, 280 and 320 nm. Twenty aliquots (100 μL each) of the appropriate stock solutions (5 mg/mL in methanol for **5b** and 5 mg/mL in acetonitrile for **5d**) were injected. After collection and evaporation of the solvent, enantiomeric excess was measured with the same conditions as the separation. Method A (for **5b**): CHIRALPAK IA (Chiral Technologies Europe, 25 cm x 0.46 cm I. D.); mobile phase: A = methanol, B = acetonitrile; isocratic solvent: 20% B; flow rate = 1 mL/min; λ = 320 nm; 100 μL injection. Method B (for **5d**): CHIRALPAK IA (Chiral Technologies Europe, 25 cm x 0.46 cm I. D.); mobile phase: A = methanol, B = acetonitrile; isocratic solvent: 30% B; flow rate = 1 mL/min; λ = 320 nm; 100 μL injection. Data were integrated and reported using OpenLAB software (Agilent Technologies). All compounds display enantiomeric excess > 99% as determined by this method. Chromatographic analyses are reported in the Supporting Information.

Volsurf+ calculations

Volsurf+ (Molecular Discovery, Perugia, Italy) was employed to compute different MIF-based[54] LogBB, a distribution parameter used to roughly assess the drug capability to cross the blood brain barrier (BBB).[46,76]

Aqueous Solubility Measurement: Turbidimetric Method

The compound under study was dissolved in DMSO (at concentration of 2.5 and 30 mg/mL for **5b** as free base, 2 and 25 mg/mL for **I**,[34] **4j** and **5a**) and added in portions to 50 mM Tris-HCl, pH 7.4, at room temperature. An Agilent 8453E UV–visible spectrophotometer equipped with a cell changer was used to detect light scattering produced by the addition of stock solutions to Tris-HCl buffer and solubility calculation were performed as previously reported[46] from a bilinear curve fit in a plot of the absorbance (y axis) versus μL of DMSO (x axis). Increased UV absorbance was measured in the 580-780 nm range. The solubility at pH 7.4 was the mean ± SEM of three independent assays and was expressed as logS (mol/L).

RP-HPLC Determination of Lipophilicity Index (log*k'*)

Log*k′* determinations were carried out using a Zorbax Eclypse-C18 4.6 mm × 250 mm, with 5 μm size particles, built on a Waters double pump HPLC system in isocratic conditions. Injection volumes were 10 μL, flow rate was 1 mL/min, and detection was performed with UV (λ = 230 and 280 nm). Samples of compounds **I**, **4j**, **5a** and **5b** were prepared in methanol at concentration 1 mM. The mobile phase was filtered through a Nylon-66 membrane 0.45 μm (Supelco, USA) before use. Log*k′* values were calculated using the following equation:

$$\log k' = \log[(t_r - t_0)/t_0]$$

where retention times (t_r) were measured at least from three separate injections, and dead time (t_0) was the retention time of KI (1 mg/mL in methanol). The mobile phase consisted of different mixtures of methanol and ammonium acetate buffer (20 mM, pH 5.0): methanol/buffer 70% (v/v), methanol/buffer 65% (v/v), methanol/buffer 60% (v/v), methanol/buffer 55% (v/v), methanol/buffer 50% (v/v), methanol/buffer 45% (v/v).

Human Monoamine Oxidases Inhibition Assays

Human monoamine oxidase inhibition assays were carried out with a fluorescence based method,[34,56] using kynuramine as non-selective MAO A and MAO B substrate. Human recombinant MAO A and

MAO B (microsomes from baculovirus infected insect cells; Sigma-Aldrich) were used. IC_{50}s for most active compounds were determined from seven concentrations ranging from 10^{-4} to 10^{-11} M. Reactions were performed in triplicates in black, round-bottomed polystyrene 96-well microtiter plates (Greiner). Samples were preincubated 20 min at 37 °C before adding MAO solutions, then incubated for additional 30 min. Fluorescence was recorded at excitation/emission wavelengths of 320/400 nm (20 nm slit width for excitation, 30 nm slit width for emission) in a 96-well microplate fluorescence reader (Tecan Infinite M100 Pro). Inhibitory activities were determined by means of non-linear regressions performed with GraphPad Prism 5.0 software and are expressed as IC_{50} (μM) or as percentage of inhibition at 10 μM. Results are the mean of three independent experiments.

Electric Eel and Equine Serum Cholinesterases Inhibition Assays

In vitro ChEs inhibition assays were performed on AChE from electric eel (463 U/mg; Sigma) and BChE from equine serum (13 U/mg; Sigma), according to the well-known spectrophotometric Ellman's method.[57] The experimental protocol for inhibition determination and kinetic studies has been adapted to a 96-well plate procedure from a previously reported method.[77] Inhibitory activities were determined by means of non-linear regressions of the response/log(concentration) curve performed with GraphPad Prism 5.0 and are reported as IC_{50} (μM) or as percentage of inhibition at 10 μM for less active compounds. Experiments were performed in triplicates in transparent, flat-bottomed polystyrene 96-well microtiter plates. Seven concentrations of inhibitor, ranging from 10^{-4} to 10^{-10} M, were used; results are the mean of three independent experiments. Kinetic studies were performed with the same test conditions, using six concentrations of substrate (from 0.033 to 0.2 mM) and four concentrations of inhibitor (0 to 8 μM). Apparent inhibition constants and kinetic parameters were calculated within the 'Enzyme kinetics' module of Prism.

Cytotoxicity assays and neuroprotection against oxidative stress insults

The cytotoxic damage produced by selected compounds and the ability to rescue cells from oxidative insults was investigated by following a protocol already described.[34] The viability of human neuroblastoma cells SH-SY5Y was determined through the MTT assay[58] in 96-well microtiter plates after 24 h incubation at 37 °C with studied compounds at concentrations 0.1, 1, 5, 10 and 50 μM and expressed as concentration responsible for 50% inhibition of cell growth (IC_{50}) or percentage of viable cells vs. untreated cells (control). The absorbance at 570 nm was determined using a Perkin Elmer 2030 multilabel reader Victor TM X3. In the same cell lines, the protective effect of selected compounds and donepezil incubated for 24 h at two different concentrations (1 and 10 μM) against three cytotoxic insults (H_2O_2 300 μM, oligomycin-A 10 μM, rotenone 20 μM) was studied.[34,78] Each compound was tested in triplicate, and the experiments were repeated three times. Cells incubated without insults and compounds were used as control. Data are determined through MTT assay and are expressed as percentage of viable cells vs. untreated cells (control). Standard error of the mean (SD) is given. Statistical significance was determined using a two-way analysis of variance (ANOVA) followed by the Bonferroni post hoc tests (GraphPad Prism vers. 5) and was assigned to $p < 0.05$ (*) and $p < 0.01$ (**).

Bi-directional Transport Studies on MDCKII-MDR1 Monolayers

As previously reported,[34,78] Madin-Darby Canine Kidney (MDCK) cells were retrovirally transfected with the human MDR1 cDNA (MDCKII-MDR1).[79,80] MDCKII-MDR1 cells were cultured in DMEM medium and seeded at a density of 100000 cell/cm^2 onto polyester 12 well Transwell inserts (pore size 0.4 μm, 12 mm diameter, apical volume 0.5 mL, basolateral volume 1.5 mL). MDCKII-MDR1 cell barrier function was verified prior to the described transport experiments by measuring trans-epithelial electrical resistance (TEER) using an EVOM apparatus and the flux of fluorescein isothiocyanate-dextran (FD4, Sigma Aldrich, Italy) (200 μg/mL) and diazepam (75 μM). The analysis of compounds (±)-**5a-b** and (±)-**5e** were performed through UV–visible (Vis) spectroscopy using a PerkinElmer double-beam UV–visible spectrophotometer Lambda Bio 20 (Milan, Italy), equipped with 10 mm path-length-matched quartz cells. Standard calibration curves were prepared at maximum absorption

wavelength of each compound using PBS as solvent and were linear ($r^2 = 0.999$) over the range of tested concentration (from 5 to 75 μM). The FD4 samples were analyzed with a Victor3 fluorimeter (Wallac Victor3, 1420 Multilabel Counter, Perkin-Elmer) at excitation and emission wavelengths of 485 and 535 nm, respectively. Each compound was tested in triplicate, and the experiments were repeated three times. Data are reported as the apparent permeability (P_{app}), in units of cm/sec, determined as indicated in the following equation:

$$P_{app} = \left(\frac{V_A}{area \times time}\right) \times \left(\frac{[drug]_{acceptor}}{[drug]_{initial}}\right)$$

where "VA" is the volume in the acceptor well, "area" is the surface area of the membrane, "time" is the total transport time, "$[drug]_{acceptor}$" is the concentration of the drug measured by UV-spectroscopy and "$[drug]_{initial}$" is the initial drug concentration in the AP or BL chamber.

Efflux ratio (ER) was calculated using the following equation: ER = P_{app}, BL-AP / P_{app}, AP-BL, where P_{app}, BL-AP is the apparent permeability of basal-to-apical transport, and P_{app}, AP-BL is the apparent permeability of apical-to-basal transport. An efflux ratio greater than 2 indicates that a test compound is likely to be a substrate for P-gp transport.

Acknowledgments

The financial support from MIUR, Italy (Grant Futuro in Ricerca 2012, RBFR12SJA8_003) is kindly acknowledged.

Corresponding Author Information

To whom correspondence should be addressed. Phone: +39-0805442780; Fax: +39-080-5442230. E-mail: marco.catto@uniba.it

Supporting Information. Applicability domain for Volsurf+ predictions; chiral-HPLC analysis on enantiomeric excess for (+)-**5b**, (−)-**5b**, (+)-**5d** and (−)-**5d**; protocols of MAOs and ChEs inhibition

assays; SMILES data (CSV). The Supporting Information is available free of charge on the ACS Publications website at DOI…….

Abbreviations Used

BBB, blood brain barrier; CAS, catalytic anionic FAD, flavin adenine dinucleotide; FD4, fluorescein isothiocyanate-dextran; MDCKII-MDR1, Madin-Darby canine kidney cells retrovirally transfected with the human MDR1 cDNA; MIF, molecular interaction field; MTDL, multi-target directed ligand; MTT, 3-(4,5-dimethylthiazol-2-yl)-2,5-diphenyltetrazolium bromide; P_{app}, apparent permeability; P_{app}, AP-BL, apparent permeability apical-to-basal; P_{app}, BL-AP, apparent permeability basal-to-apical; PAS, peripheral anionic binding site; P-gp, P-glycoprotein; ROS, reactive oxygen species; SAR, structure-activity relationships; TEER, trans-epithelial electrical resistance.

References

1 Wimo, A.; Jonsson, L.; Bond, J.; Prince, M.; Winblad, B. The Worldwide Economic Impact of Dementia 2010. *Alzheimer's Dementia* **2013**, *9*, 1-11.

2 Querfurth, H. W.; LaFerla, F. M. Alzheimer's Disease. *N. Engl. J. Med.* **2010**, *362*, 329-344.

3 Cummings, J. L.; Morstorf, T.; Zhong, K. Alzheimer's Disease Drug-development Pipeline: Few Candidates, Frequent Failures. *Alzheimer's Res. Ther.* **2014**, *6*, 37.

4 Berk, C.; Sabbagh, M. N. Successes and Failures for Drugs in Late-stage Development for Alzheimer's Disease. *Drugs Aging* **2013**, *10*, 783-792.

5 Narayan, P.; Ehsani, S.; Lindquist, S. Combating Neurodegenerative Disease with Chemical Probes and Model Systems. *Nat. Chem. Biol.* **2014**, *10*, 911-920.

6 Bush, A. I. The Metal Theory of Alzheimer's Disease. *J. Alzheimer's Dis.* **2013**, *33*, S277-S281.

7 Zhao, Y.; Zhao, B. Oxidative Stress and the Pathogenesis of Alzheimer's Disease. *Oxid. Med. Cell. Longevity* **2013**, *2013*, 316523.

8 Terry, Jr. A. V.; Buccafusco, J. J. The Cholinergic Hypothesis of Age and Alzheimer's Disease-related Cognitive Deficits: Recent Challenges and Their Implications for Novel Drug Development. *J. Pharmacol. Exp. Ther.* **2003**, *306*, 821-827.

9 Johnson, J. W.; Kotermanski, S. E. Mechanism of Action of Memantine. *Curr. Opin. Pharmacol.* **2006**, *6*, 61-67.

10 Muñoz-Torrero, D. Acetylcholinesterase Inhibitors as Disease Modifying Therapies for Alzheimer's Disease. *Curr. Med. Chem.* **2008**, *15*, 2433−2455.

11 Zimmermann, G. R.; Lehár, J.; Keith, C. T. Multi-target Therapeutics: When the Whole is Greater than the Sum of the Parts. *Drug Discovery Today* **2007**, *12*, 34-42.

12 Leon, R.; Garcia, A. G.; Marco-Contelles, J. Recent Advances in the Multitarget-Directed Ligands Approach for the Treatment of Alzheimer's Disease. *Med. Res. Rev.* **2013**, *33*, 139-189.

13 Lee, S.; Zheng, X.; Krishnamoorthy, J.; Savelieff, M. G.; Park, H. M.; Brender, J. R.; Kim, J. H.; Derrick, J. S.; Kochi, A.; Lee, H. J.; Kim, C.; Ramamoorthy, A.; Bowers, M. T.; Lim, M. H. Rational Design of a Structural Framework with Potential Use to Develop Chemical Reagents that Target and Modulate Multiple Facets of Alzheimer's Disease. *J. Am. Chem. Soc.* **2014**, *136*, 299-310.

14 Prati, F.; De Simone, A.; Bisignano, P.; Armirotti, A.; Summa, M.; Pizzirani, D.; Scarpelli, R.; Perez, D. I.; Andrisano, V.; Perez-Castillo, A.; Monti, B.; Massenzio, F.; Polito, L.; Racchi, M.; Favia, A. D.; Bottegoni, G.; Ana Martinez, A.; Bolognesi, M. L.; Cavalli, A. Multitarget Drug Discovery for Alzheimer's Disease: Triazinones as BACE-1 and GSK-3β Inhibitors. *Angew. Chem. Int. Ed.* **2015**, *54*, 1578–1582.

15 Zheng, H.; Youdim, M. B. H.; Fridkin, M. Site-activated Chelators Targeting Acetylcholinesterase and Monoamine Oxidase for Alzheimer's Therapy. *ACS Chem. Biol.* **2010**, *5*, 603-610.

16 Rochais, C.; Lecoutey, C.; Gaven, F.; Giannoni, P.; Hamidouche, K.; Hedou, D.; Dubost, E.; Genest, D.; Yahiaoui, S.; Freret, T.; Bouet, V.; Dauphin, F.; Sopkova de Oliveira Santos, J.; Ballandonne, C.; Corvaisier, S.; Malzert-Fréon, A.; Legay, R.; Boulouard, M.; Claeysen, S.; Dallemagne, P. Novel Multitarget-directed Ligands (MTDLs) with Acetylcholinesterase (AChE) Inhibitory and Serotonergic Subtype 4 Receptor (5-HT4R) Agonist Activities as Potential Agents against Alzheimer's Disease: the Design of Donecopride. *J. Med. Chem.* **2015**, *58*, 3172-3187.

17 Pau, A.; Catto, M.; Pinna, G.; Frau, S.; Murineddu, G.; Asproni, B.; Curzu, M. M.; Pisani, L.; Leonetti, F.; Loza, M. I.; Brea, J.; Pinna, G. A.; Carotti, A. Multitarget-directed Tricyclic Pyridazinones

as Ligands of Selected G-protein Coupled Receptors and Inhibitors of Cholinesterases. *ChemMedChem* **2015**, *10*, 1054-1070.

18 Fernández-Bachiller, M. I.; Pérez, C.; Monjas, L.; Rademann, J.; Rodríguez-Franco, M. I. New Tacrine−4-Oxo-4H-chromene Hybrids as Multifunctional Agents for the Treatment of Alzheimer's Disease, with Cholinergic, Antioxidant, and β-Amyloid-Reducing Properties. *J. Med. Chem.* **2012**, *55*, 1303−1317.

19 Chen, Y.; Sun, J.; Fang, L.; Liu, M.; Peng, S.; Liao, H.; Lehmann, J.; Zhang, Y. Tacrine−Ferulic Acid−Nitric Oxide (NO) Donor Trihybrids as Potent, Multifunctional Acetyl- and Butyrylcholinesterase Inhibitors. *J. Med. Chem.* **2012**, *55*, 4309−4321.

20 Fang, L.; Appenroth, D.; Decker, M.; Kiehntopf, M.; Lupp, A.; Peng, S.; Fleck, C.; Zhang, Y.; Lehmann, J. NO-Donating Tacrine Hybrid Compounds Improve Scopolamine-Induced Cognition Impairment and Show Less Hepatotoxicity *J. Med. Chem.* **2008,** *51,* 7666–7669.

21 Dvira, H.; Silman, I.; Harel, M.; Rosenberry, T. L.; Sussman, J. L. Acetylcholinesterase: From 3D Structure to Function. *Chem. Biol. Interact.* **2010**, *187*, 10–22.

22 Harel, M.; Schalk, I.; Ehret-Sabatier, L.; Bouet, F.; Goeldner, M.; Hirth, C.; Axelsen, P. H.; Silman, I.; Sussman, J. L. Quaternary Ligand Binding to Aromatic Residues in the Active-site Gorge of Acetylcholinesterase. *Proc. Nat. Acad. Sci. U.S.A.* **1993**, *90*, 9031–9035.

23 Inestrosa, N. C.; Alvarez, A.; Pérez, C. A.; Moreno, R. D.; Vicente, M.; Linker, C.; Casanueva, O. I.; Soto, C.; Garrido, J. Acetylcholinesterase Accelerates Assembly of Amyloid-β-peptides into Alzheimer's Fibrils: Possible Role of the Peripheral Site of the Enzyme. *Neuron* **1996**, *16*, 881-891.

24 Lockridge O. Review of Human Butyrylcholinesterase Structure, Function, Genetic Variants, History of Use in the Clinic, and Potential Therapeutic Uses. *Pharmacol. Ther.* **2015**, *148*, 34-46.

25 Lane, R. M.; Potkin, S. G., Enz, A. Targeting Acetylcholinesterase and Butyrylcholinesterase in Dementia. *Int. J. Neuropsychopharmacol.* **2006**, *9*, 101-124.

26 Giacobini E. Selective Inhibitors of Butyrylcholinesterase: a Valid Alternative for Therapy of Alzheimer's Disease? *Drugs Aging* **2001**, *18*, 891-898.

27 Riederer, P.; Danielczyk, W.; Gruenblatt, E. Monoamine Oxidase-B Inhibition in Alzheimer's Disease. *Neurotoxicology* **2004**, *1*, 271-277.

28 De Colibus, L.; Li, M.; Binda, C.; Lustig, A.; Edmondson, D. E.; Mattevi, A. Three-Dimensional Structure of Human Monoamine Oxidase A (MAO A): Relation to the Structures of Rat MAO A and Human MAO B. *Proc. Natl. Acad. Sci. U.S.A.* **2005**, *102*, 12684−12689.

29 Binda, C.; Newton-Vinson, P.; Hubalek, F.; Edmondson, D. E.; Mattevi, A. Structure of Human Monoamine Oxidase B, a Drug Target for the Treatment of Neurological Disorders. *Nat. Struct. Mol. Biol.* **2002**, *9*, 22−26.

30 Rapaport, M. H. Dietary Restrictions and Drug Interactions with Monoamine Oxidase Inhibitors: the State of the Art. *J. Clin. Psychiatry* **2007**, *68*, 42-46.

31 Wimbiscus, M.; Kostenko, O.; Malone, D. MAO Inhibitors: Risks, Benefits, and Lore. *Cleve. Clin. J. Med.* **2010**, *77*, 859-882.

32 Barnham, K. J.; Masters, C. L.; Bush, A. I. Neurodegenerative Diseases and Oxidative Stress. *Nat. Rev. Drug Discovery* **2004**, *3*, 205-214.

33 Tonelli, M.; Catto, M.; Tasso, B.; Novelli, F.; Canu, C.; Iusco, G.; Pisani, L.; De Stradis, A.; Sparatore, A.; Boido, V.; Carotti, A.; Sparatore, F. Multitarget Therapeutic Leads for Alzheimer's disease. Quinolizidinyl Derivatives of Bi- and Tri-cyclic Systems as Dual Inhibitors of Cholinesterases and Aβ Aggregation. *ChemMedChem* **2015**, *10*, 1040-1053.

34 Farina, R.; Pisani, L.; Catto, M.; Nicolotti, O.; Gadaleta, D.; Denora, N.; Soto-Otero, R.; Mendez-Alvarez, E.; Passos, C. S.; Muncipinto, G.; Altomare, C. D.; Nurisso, A.; Carrupt, P. A.; Carotti, A. Structure-Based Design and Optimization of Multitarget-Directed 2*H*□Chromen-2-one Derivatives as Potent Inhibitors of Monoamine Oxidase B and Cholinesterases. *J. Med. Chem.* **2015**, *58*, 5561−5578.

35 Matos, M. J.; Terán, C.; Pérez-Castillo, Y.; Uriarte, E.; Santana, L.; Viña, D. Synthesis and Study of a Series of 3-Arylcoumarins as Potent and Selective Monoamine Oxidase B Inhibitors. *J. Med. Chem.* **2011**, *54*, 7127-7137.

36 Mertens, M. D.; Hinz, S.; Müller, C. E.; Gütschow, M. Alkynyl–coumarinyl Ethers as MAO-B Inhibitors. *Bioorg. Med. Chem.* **2014**, *22*, 1916–1928.

37 Secci, D.; Carradori, S.; Bolasco, A.; Chimenti, P.; Yáñez, M.; Ortuso, F.; Alcaro, S. Synthesis and Selective Human Monoamine Oxidase Inhibition of 3-Carbonyl, 3-Acyl, and 3-Carboxyhydrazido Coumarin Derivatives. *Eur. J. Med. Chem.* **2011**, *46*, 4846-4852.

38 Patil, P. O.; Bari, S. B.; Firke, S. D.; Deshmukh, P. K.; Donda, S. T.; Patil, D. A. A Comprehensive Review on Synthesis and Designing Aspects of Coumarin Derivatives as Monoamine Oxidase Inhibitors for Depression and Alzheimer's Disease. *Bioorg. Med. Chem.* **2013**, *21*, 2434-2450.

39 Delogu, G.; Picciau, C.; Ferino, G.; Quezada, E.; Podda, G.; Uriarte, E.; Viña, D. Synthesis, Human Monoamine Oxidase Inhibitory Activity and Molecular Docking Studies of 3-Heteroaryl Coumarin Derivatives. *Eur. J. Med. Chem.* **2011**, *46*, 1147-1152.

40 Catto, M.; Pisani, L.; Leonetti, F.; Nicolotti, O.; Pesce, P.; Stefanachi, A.; Cellamare, S.; Carotti, A. Design, Synthesis and Biological Evaluation of Coumarin Alkylamines as Potent and Selective Dual Binding Site Inhibitors of Acetylcholinesterase. *Bioorg. Med. Chem.* **2013**, *21*, 146–152.

41 Alipour, M.; Khoobi, M.; Moradi, A.; Nadri, H;.; Moghadam, F. H.; Emami, S.; Hasanpour, Z.; Foroumadi, A.; Shafiee, A. Synthesis and Anti-cholinesterase Activity of New 7-Hydroxycoumarin Derivatives. *Eur. J. Med. Chem.* **2014**, *23*, 536-544.

42 Pisani, L.; Catto, M.; Giangreco, I.; Leonetti, F.; Nicolotti, O.; Stefanachi, A.; Cellamare, S.; Carotti, A. Design, Synthesis and Biological Evaluation of Coumarin Derivatives Tethered to an Edrophonium-like Fragment as Highly Potent and Selective Dual Binding Site Acetylcholinesterase Inhibitors. *ChemMedChem* **2010**, *5*, 1616-1630.

43 Wang, Z.-M.; Li, X.-M.; Xue, G.-M.; Xu, W.; Wang, X.-B.; Kong, L.-Y. Synthesis and Evaluation of 6-Substituted 3-Arylcoumarin Derivatives as Multifunctional Acetylcholinesterase/monoamine Oxidase B Dual Inhibitors for the Treatment of Alzheimer's Disease. *RSC Advances* **2015**, *5*, 104122-104137.

44 Xie, S.-S.; Wang, X.; Jiang, N.; Yu, W.; Wang, K. D. G.; Lan, J.-S.; Li, Z.-R.; Kong, L.-Y. Multi-target Tacrine-coumarin Hybrids: Cholinesterase and Monoamine Oxidase B Inhibition Properties against Alzheimer's Disease. *Eur. J. Med. Chem.* **2015**, *95*, 153-165.

45 Jameel, E.; Umar, T.; Kumar, J.; Hoda, N. Coumarin: A Privileged Scaffold for the Design and Development of Antineurodegenerative Agents. *Chem. Biol. Drug Des.* **2016**, *87*, 21-38.

46 Pisani, L.; Muncipinto, G.; Miscioscia, T. F.; Nicolotti, O.; Leonetti, F.; Catto, M.; Caccia, C.; Salvati, P.; Soto-Otero, R.; Mendez-Alvarez, E.; Passeleu, C.; Carotti, A. Discovery of a Novel Class of Potent Coumarin Monoamine Oxidase B Inhibitors: Development and Biopharmacological Profiling of 7-[(3-Chlorobenzyl)oxy]-4-[(methylamino)methyl]-2H-chromen-2-one Methanesulfonate (NW-1772) as a Highly Potent, Selective, Reversible, and Orally Active Monoamine Oxidase B Inhibitor. *J. Med. Chem.* **2009**, *52*, 6685–6706.

47 Pisani, L.; Barletta, M.; Soto-Otero, R.; Nicolotti, O.; Mendez-Alvarez, E.; Catto, M.; Introcaso, A.; Stefanachi, A.; Cellamare, S.; Altomare, C.; Carotti, A. Discovery, Biological Evaluation, and Structure−Activity and −Selectivity Relationships of 6′-Substituted (E)-2-(Benzofuran-3(2*H*)-ylidene)-*N*-methylacetamides, a Novel Class of Potent and Selective Monoamine Oxidase Inhibitors. *J. Med. Chem.* **2013**, *56*, 2651–2664.

48 Catto, M.; Nicolotti, O.; Leonetti, F.; Carotti, A.; Favia, A. D.; Soto-Otero, R.; Mendez-Alvarez, E.; Carotti, A. Structural Insights into Monoamine Oxidase Inhibitory Potency and Selectivity of 7-Substituted Coumarins from Ligand- and Target-Based Approaches. *J. Med. Chem.* **2006**, *49*, 4912−4925.

49 Carotti, A.; Altomare, C.; Catto, M.; Gnerre, C.; Summo, L.; De Marco, A.; Rose, S.; Jenner, P.; Testa, B. Lipophilicity Plays a Major Role in Modulating Monoamine Oxidase B (MAO-B). Inhibition by 7-Substituted Coumarins. *Chem. Biodiversity* **2006**, *3*, 134-144.

50 Pisani, L.; Catto, M.; Nicolotti, O.; Grossi, G.; Di Braccio, M.; Soto-Otero, R.; Mendez-Alvarez, E.; Stefanachi, A.; Gadaleta, D.; Carotti, A. Fine Molecular Tuning at Position 4 of 2*H*-Chromen-2-one Derivatives in the Search of Potent and Selective Monoamine Oxidase B Inhibitors. *Eur. J. Med. Chem.* **2013**, *70*, 723–739.

51 Cheung, J.; Rudolph, M. J.; Burshteyn, F.; Cassidy, M. S.; Gary, E. N.; Love, J.; Franklin, M. C.;, Height, J. J. Structures of Human Acetylcholinesterase in Complex with Pharmacologically Important Ligands. *J. Med. Chem.* **2012**, *55*, 10282-10286.

52 Pisani, L.; Farina, R.; Nicolotti, O.; Gadaleta, D.; Soto-Otero, R.; Catto, M.; Di Braccio, M.; Mendez-Alvarez, E.; Carotti, A. In Silico Design of Novel 2*H*-Chromen-2-one Derivatives as Potent and Selective MAO-B Inhibitors. *Eur. J. Med. Chem.* **2015**, *89*, 98-105.

53 Bruhlmann, C.; Ooms, F.; Carrupt, P.A.; Testa, B.; Catto, M.; Leonetti, F.; Altomare, C.; Carotti, A. Coumarins Derivatives as Dual Inhibitors of Acetylcholinesterase and Monoamine Oxidase. *J. Med. Chem.* **2001**, *44*, 3195-3198.

54 Cruciani, G.; Crivori, P.; Carrupt, P. A.; Testa, B. Molecular Fields in Quantitative Structure-Permeation Relationships: The VolSurf Approach. *J. Mol. Struct.* **2000**, *503*, 17–30.

55 Gnerre, C.; Catto, M.; Leonetti, F.; Weber, P.; Carrupt, P.-A.; Altomare, C.; Carotti, A.; Testa, B. Inhibition of Monoamine Oxidases by Functionalized Coumarin Derivatives: Biological Activities, QSARs, and 3D-QSARs. *J. Med. Chem.* **2000**, *43*, 4747−4758.

56 Novaroli, L.; Daina, A.; Favre, E.; Bravo, J.; Carotti, A.; Leonetti, F.; Catto, M.; Carrupt, P.-A.; Reist, M. Impact of Species-dependent Differences on Screening, Design, and Development of MAO-B Inhibitors. *J. Med. Chem.* **2006**, *49*, 6264-6272.

57 Ellman, G. L.; Courtney, K. D.; Andres, V., Jr.; Feartherstone, R. M. A New and Rapid Colorimetric Determination of Acetylcholinesterase Activity. *Biochem. Pharmacol.* **1961**, *7*, 88–95.

58 Denizot, F.; Lang, R. Rapid Colorimetric Assay for Cell Growth and Survival. Modifications to the Tetrazolium Dye Procedure Giving Improved Sensitivity and Reliability. *J. Immunol. Methods* **1986**, *89*, 271-277.

59 Denora, N.; Laquintana, V.; Lopalco, A., Iacobazzi, R. M., Lopedota, A., Cutrignelli, A., Iacobellis, G., Annese, C., Cascione, M., Leporatti, S., Franco, M. In vitro targeting and imaging the translocator protein TSPO 18-kDa through G(4)-PAMAM-FITC labeled dendrimer. *J. Controlled Release* **2013**, *172*, 1111-1125.

60 Crivori, P.; Cruciani, G.; Carrupt, P. A.; Testa, B. Predicting Blood-Brain Barrier Permeation from Three-Dimensional Molecular Structure. *J. Med. Chem.* **2000**, *43*, 2204–2216.

61 a) Tropsha, A.; Gramatica, P.; Gombar, V. The Importance of Being Earnest: Validation is the Absolute Essential for Successful Application and Interpretation of QSPR Models. *Mol. Inform.* **2003**, *22*, 69-77; b) Eriksson, L.; Jaworska, J.; Worth, A.; Cronin, M. T. D., McDowell, R. M.; Gramatica, P. Methods for Reliability and Uncertainty Assessment and for Applicability Evaluations of Classification- and Regression- Based QSARs. *Environ. Health Perspect.* **2003**, *111*, 1351–1375.

62 Li, N.; Ragheb, K.; Lawler, G.; Sturgis, J.; Rajwa, B; Melendez, A. J.; Robinson, J. P. Mitochondrial Complex I Inhibitor Rotenone Induces Apoptosis through Enhancing Mitochondrial Reactive Oxygen Species Production. *J. Biol. Chem.* **2003**, *278*, 8516–8525.

63 Shchepina, L. A.; Pletjushkina, O. Y.; Avetisyan, A. V.; Bakeeva, L. E.; Fetisova, E. K.; Izyumov, D. S.; Saprunova, V. B.; Vyssokikh, M. Y.; Chernyak, B. V.; Skulachev, V. P. Oligomycin, Inhibitor of the F_0 Part of H^+-ATP-synthase, Suppresses the TNF-induced Apoptosis. *Oncogene* **2002**, *21*, 8149-8157.

64 Rankovic, Z. CNS Drug Design: Balancing Physicochemical Properties for Optimal Brain Exposure. *J. Med. Chem.* **2015**, *58*, 2584–2608.

65 Pajouhesh, H.; Lenz, G. R. Medicinal Chemical Properties of Successful Central Nervous System Drugs. *NeuroRx* **2005**, *2*, 541−553.

66 Fernandez-Bachiller, M. I.; Perez, C.; Monjas, L.; Rademann, J.; Rodríguez-Franco, M. I. New Tacrine−4-Oxo-4*H*-chromene Hybrids as Multifunctional Agents for the Treatment of Alzheimer's Disease, with Cholinergic, Antioxidant, and β-Amyloid-Reducing Properties. *J. Med. Chem.* **2012**, *55*, 1303 −1317.

67 Otto, R.; Penzis, R.; Gaube, F.; Adolph, O.; Fohr, K. J.; Warncke, P.; Robaa, D.; Appenroth, D.; Fleck, C.; Enzensperger, C.; Lehmann, J.; Winckler, T. Evaluation of Homobivalent Carbolines as

Designed Multiple Ligands for the Treatment of Neurodegenerative Disorders. *J. Med. Chem.* **2015**, *58*, 6710 −6715.

68 Di Pietro, O.; Pérez-Areales, F. J.; Juárez-Jiménez, J.; Espargaró, A.; Clos, M. V.; Pérez, B.; Lavilla, R.; Sabaté, R.; Luque, F. J.; Muñoz-Torrero, D. Tetrahydrobenzo[h][1,6]naphthyridine-6-chlorotacrine Hybrids as a New Family of Anti-Alzheimer Agents Targeting β-Amyloid, Tau, and Cholinesterase Pathologies. *Eur. J. Med. Chem.* **2014**, *84*, 107-117.

69 Viayna, E.; Sola, I.; Manuela Bartolini, M.; De Simone, A.; Tapia-Rojas, C.; G. Serrano, F. G.; Sabate, R.; Juarez-Jimenez, J.; Perez, B.; Luque, F. J.; Andrisano, V.; Clos, M. V.; Inestrosa, N. C.; Muñoz-Torrero, D. Synthesis and Multitarget Biological Profiling of a Novel Family of Rhein Derivatives As Disease-Modifying Anti-Alzheimer Agents. *J. Med. Chem.* **2014**, *57*, 2549−2567.

70 Wu, M.; Esteban, G.; Brogi, S.; Shionoya, M.; Wang, L.; Campiani, G.; Unzeta, M.; Inokuchi, T; Butini, S.; Marco-Contelles, J. Donepezil-like Multifunctional Agents: Design, Synthesis, Molecular Modeling and Biological Evaluation. *Eur. J. Med. Chem.* **2015**, http://dx.doi.org/10.1016/j.ejmech.2015.10.001.

71 Wang, L.; Esteban, G.; Ojima, M.; Bautista-Aguilera, O. M.; Inokuchi, T.; Moraleda, I.; Iriepa, I.; Samadi, A.; Youdim, M. B. H.; Romero, A.; Soriano, E.; Herrero, R.; Fernández Fernández, A.P.; Martínez-Murillo, R.; Marco-Contelles, J.; Unzeta, M. Donepezil + Propargylamine + 8-Hydroxyquinoline Hybrids as New Multifunctional Metal-chelators, ChE and MAO Inhibitors for the Potential Treatment of Alzheimer's Disease. *Eur. J. Med. Chem.* **2014**, *80*, 543-561.

72 Weinstock, M.; Bejar, C.; Wang, R. H.; Poltyrev, T.; Gross, A.; Finberg, J. P.; Youdim, M. B. TV3326, a Novel Neuroprotective Drug with Cholinesterase and Monoamine Oxidase Inhibitory Activities for the Treatment of Alzheimer's Disease. *J. Neural Transm. Suppl.* **2000**, *60*, 157-169.

73 Sterling, J.; Herzig, Y.; Goren, T.; Finkelstein, N.; Lerner, D.; Goldenberg, W.; Miskolczi, I.; Molnar, S.; Rantal, F.; Tamas, T.; Toth, G.; Zagyva, A.; Zekany, A.; Lavian, G.; Gross, A.; Friedman, R.; Razin, M.; Huang, W.; Krais, B.; Chorev, M.; Youdim, M.B.H.; Weinstock, M. Novel Dual Inhibitors of AChE and MAO Derived from Hydroxy Aminoindan and Phenethylamine as Potential Treatment for Alzheimer's Disease. *J. Med. Chem.* **2002**, *45*, 5260-5279.

74 http://www.businesswire.com/news/home/20150728005672/en/Avraham-Pharmaceuticals-Announces-Successful-Interim-Results-Phase, accessed July 28, 2015.

75 Anderson, M. C.; Hasan, F.; McCrodden, J. M.; Tipton, K. F. Monoamine Oxidase Inhibitors and the Cheese Effect. *Neurochem. Res.* **1993**, *18*, 1145−1149.

76 Lobell, M.; Molnár, L.; Keserü, G. M. Recent Advances in the Prediction of Blood–brain Partitioning from Molecular Structure. *J. Pharm. Sci.* **2003**, *92*, 360–370.

77 Conejo-García, A.; Pisani, L.; Núñez, M. d. C.; Catto, M.; Nicolotti, O.; Leonetti, F.; Campos, J. M.; Gallo, M. A.; Espinosa, A.; Carotti, A. Homodimeric bis-Quaternary Heterocyclic Ammonium Salts as Potent Acetyl- and Butyryl-cholinesterase Inhibitors: A Systematic Investigation of the Influence of Linker and Cationic Heads Over Affinity and Selectivity. *J. Med. Chem.* **2011**, *54*, 2627-2645.

78 Pisani, L.; Farina, R.; Soto-Otero, R.; Denora, N.; Mangiatordi, G. F.; Nicolotti, O.; Mendez-Alvarez, E.; Altomare, C. D.; Catto, M.; Carotti, A. Searching for Multi-Targeting Neurotherapeutics against Alzheimer 's: Discovery of Potent AChE-MAO B Inhibitors through the Decoration of the 2*H* Chromen-2-one Structural Motif. *Molecules* **2016**, *21*, doi:10.3390/molecules21030362.

79 Denora, N.; Laquintana, V.; Trapani, A.; Lopedota, A.; Latrofa, A.; Gallo, J. M.; Trapani, G. Translocator Protein (TSPO) Ligand-Ara-C (Cytarabine) Conjugates as a Strategy to Deliver Antineoplastic Drugs and to Enhance Drug Clinical Potential. *Mol. Pharm.* **2010**, *7*, 2255-2269.

80 Denora, N.; Cassano, T.; Laquintana, V.; Lopalco, A.; Trapani, A.; Cimmino, C. S.; Laconca, L.; Giuffrida, A.; Trapani, G. Novel Codrugs with GABAergic Activity for Dopamine Delivery in the Brain. *Int. J. Pharm.* **2012**, *437*, 221-231.

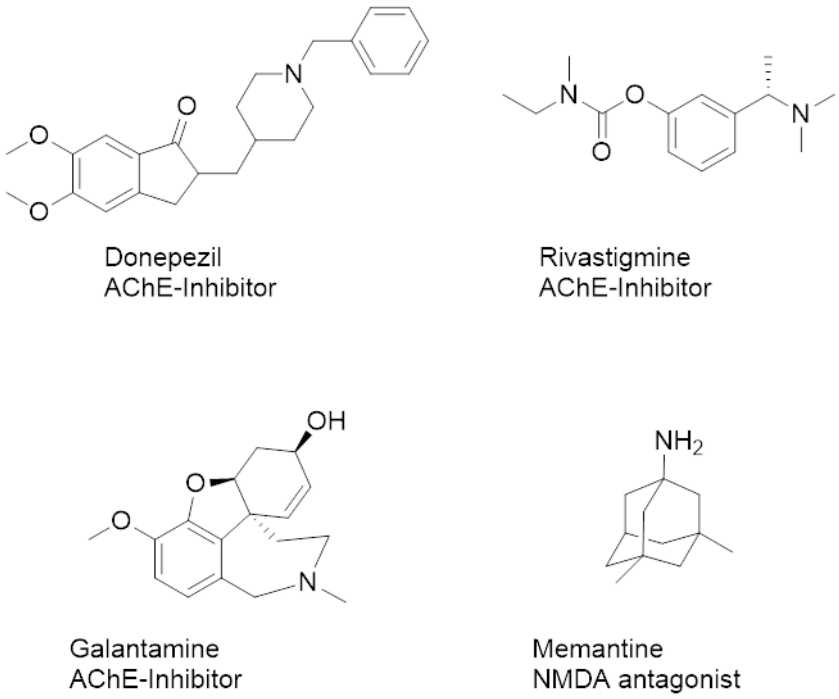

Chart 1. Approved Drugs for AD (common name, mechanism of action).

Scheme 1. Synthesis of compounds **4a**-**m**, (±)-**5a**-**i**[a]

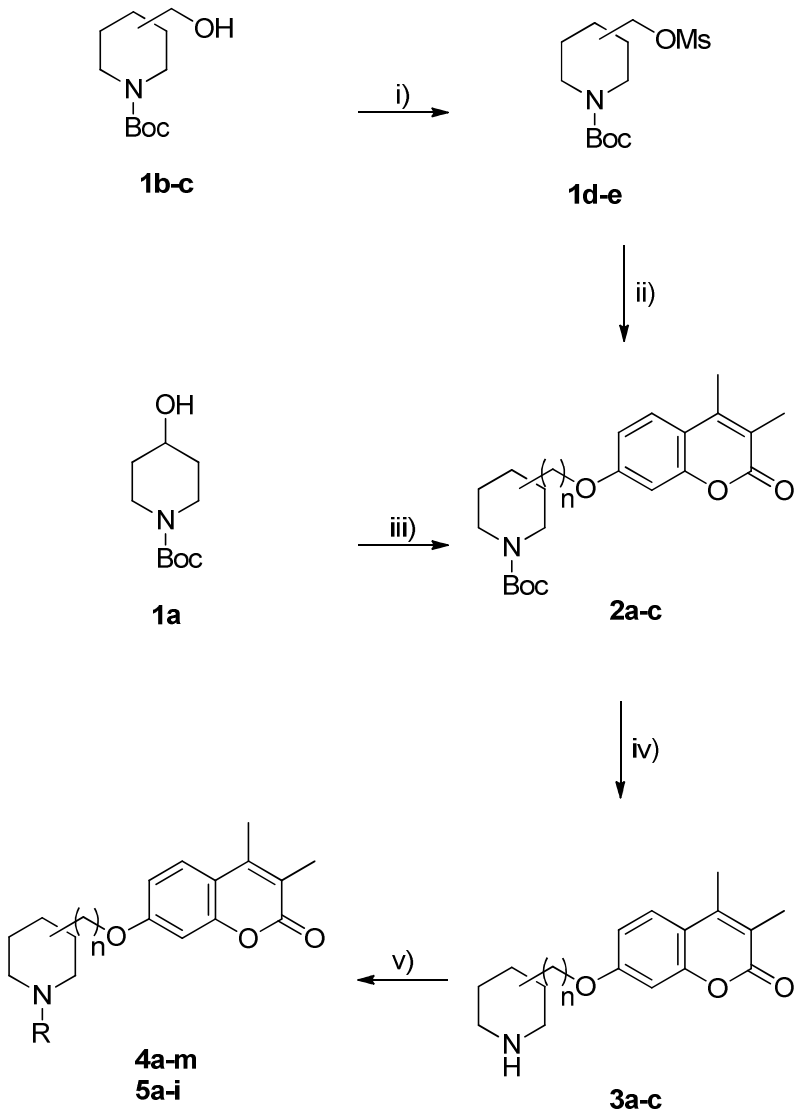

[a] Reagents and conditions: i) methanesulfonyl chloride, triethylamine, CH_2Cl_2, 3 h, room temperature; ii) 3,4-dimethyl-7-hydroxycoumarin, triethylamine, Cs_2CO_3, dry DMF, 72 h, 70 °C; iii) 3,4-dimethyl-7-hydroxycoumarin, ADDP, PPh_3, triethylamine, anhydrous CH_2Cl_2, 15 h, room temperature; iv) trifluoroacetic acid, CH_2Cl_2, 1 h, 0 °C to room temperature; v) for **4a**, **4i** and **5a**: methyl iodide, anhydrous K_2CO_3, acetone, 6 h, room temperature; for **4b**-**h**, **4j**-**m** and **5b**-**h**: butyl iodide (for **4b**) or substituted benzyl bromide, anhydrous K_2CO_3, acetone, 30 min, 130 °C, MW; for **5i**: 3,4-dimethoxybenzaldehyde, sodium triacetoxyborohydride, 1,2-dichloroethane, 15 h, room temperature.

Scheme 2. Synthesis of compounds **7a-b**[a]

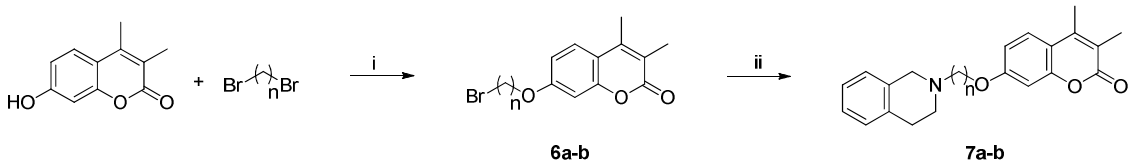

[a] Reagents and conditions: i) dibromoalkyl derivative, anhydrous K_2CO_3, acetone, 130 °C, 30 min, MW; ii) 1,2,3,4-tetrahydroisoquinoline, anhydrous K_2CO_3, acetone, 130 °C, 30 min, MW.

Table 1. MAOs and ChEs inhibition data for compounds **4a-m**, (±)-**5a-i** and **7a-b**

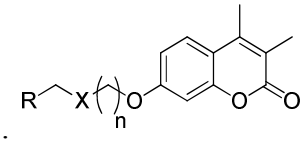

compd	n	X	R	logBBB[a]	IC$_{50}$, μM (or inhibition % at 10 μM)			
					MAO A[b]	MAO B[b]	AChE[c]	BChE[d]
4a	0		H	0.586	11.7±3.1	0.274±0.053	1.30 ±0.12	11±1%
4b	0		*n*-Pr	0.707	23.9±2.0	1.409±0.452	0.99 ±0.17	35±3%
4c	0		Ph	0.609	3.59±0.17	0.445±0.049	0.78 ±0.11	9.57 ±0.18
4d	0		3-ClPh	0.530	0.87±0.45	0.285±0.026	1.08 ±0.06	28±2%
4e	0		4-ClPh	0.618	1.59±0.01	0.876±0.021	1.55 ±0.24	29±2%
4f	0		4-CNPh	0.235	1.29±0.39	0.656±0.144	0.97 ±0.16	48±1%
4g	0		Bn	0.717	12.4±0.1	2.49±0.38	1.65 ±0.49	1.77 ±0.37
4h	0		PhCO	0.425	1.96±0.13	0.114±0.020	3.78 ±0.52	45±3%
4i[d]	1		H	0.471	16.6±1.8	0.297±0.059	0.68 ±0.16	14±1%
4j[d]	1		Ph	0.547	2.41±1.51	0.105 ±0.001	1.66 ±0.42	4.72 ±0.71
4k[d]	1		3-ClPh	0.548	0.70±0.12	0.089±0.002	1.03 ±0.03	6.07 ±0.11
4l[d]	1		4-ClPh	0.569	37%	0.614±0.085	9.57 ±0.12	19±3%
4m[d]	1		4-CNPh	0.122	10.1±0.3	0.549±0.020	1.81 ±0.77	27±3%
(±)-**5a**[d]	1		H	0.551	9.33±0.21	0.137±0.022	0.80 ±0.08	19±1%
(±)-**5b**[d]	1		Ph	0.477	2.81±0.80	0.030±0.005	1.03 ±0.05	3.41±0.19
(+)-**5b**	1		Ph	0.477	3.84±0.15	0.023±0.003	1.80±0.29	2.91±0.03
(-)-**5b**	1		Ph	0.477	2.30±0.47	0.195±0.076	0.78±0.01	8.08±0.48
(±)-**5c**[d]	1		3-ClPh	0.457	0.98±0.08	0.036±0.014	1.17 ±0.45	4.69 ±0.39
(±)-**5d**[d]	1		3-BrPh	0.557	0.81±0.16	0.110±0.021	1.91 ±0.65	30±3%
(+)-**5d**	1		3-BrPh	0.557	0.54±0.20	0.026±0.005	3.23 ±0.23	36±1%
(-)-**5d**	1		3-BrPh	0.557	1.11±0.10	0.196±0.008	1.72 ±0.04	26±2%
(±)-**5e**[d]	1		4-FPh	0.494	1.11±0.27	0.163±0.002	1.46 ±0.45	3.69 ±0.31
(±)-**5f**[d]	1		4-ClPh	0.557	0.822±0.002	0.050±0.011	2.89 ±0.72	5.90 ±0.21
(±)-**5g**[d]	1		4-MeSO$_2$Ph	0.011	0.21±0.03	0.113±0.021	0.85 ±0.02	10±1%

(±)-**5h**[d]	1	4-CNPh	0.148	4.51±1.47	0.034±0.004	2.80 ±0.35	36±1%
(±)-**5i**	1	3,4-diMeOPh	0.306	1.72±0.06	0.090±0.006	2.21 ±0.52	6.04 ±0.25
7a[d]	3	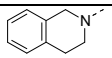	0.451	2.68±0.85	0.298±0.003	1.22 ±0.13	0.95±0.10
7b[d]	4	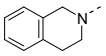	0.476	2.24±0.28	0.612±0.040	1.15 ±0.01	2.61±0.25
	donepezil					0.021 ±0.002	2.31±0.12
	clorgyline			0.0025 ±0.0003	2.55±0.55		
	pargyline			10.9±0.6	2.69±0.48		

[a] Calculated with Volsurf+ package (Molecular Discovery, Perugia, Italy). [b] Human recombinant MAOs on Supersomes. [c] AChE from Electric eel. [d] BChE from horse serum. [e] Tested as hydrochloride salt.

Table 2. Bi-directional transport across MDCKII-MDR1 cells of compounds (±)-**5a-b** and (±)-**5d**.

compd	P_{app}, AP-BL (cm/sec)	P_{app}, BL-AP (cm/sec)	ER[a]
(±)-**5a**	$2.23 \pm 0.11*10^{-5}$	$2.02 \pm 0.7*10^{-5}$	0.90
(±)-**5b**	$2.43 \pm 0.65*10^{-5}$	$1.48 \pm 0.30*10^{-5}$	0.61
(±)-**5d**	$8.40 \pm 0.25*10^{-7}$	$2.16 \pm 0.22*10^{-6}$	2.56
diazepam	$2.58 \pm 0.03*10^{-5}$	$2.53 \pm 0.05*10^{-5}$	0.98
FD-4	$8.94 \pm 0.15*10^{-6}$	$8.03 \pm 0.20*10^{-6}$	0.89

[a] Efflux ratio (ER) was calculated using the following equation: ER = P_{app}, BL-AP / P_{app}, AP-BL, where P_{app}, BL-AP is the apparent permeability of basal-to-apical transport, and P_{app}, AP-BL is the apparent permeability of apical-to-basal transport. An efflux ratio greater than 2 indicates that a test compound is likely to be a substrate for P-gp transport.

Table 3. Aqueous Solubility and Lipophilicity Index of Compounds **I**,[34] **4j**, (±)-**5a** and (±)-**5b**.

compd	LogS (pH 7.4) [a]	Log*k*' [b]	cLogP [c]
I[34]	-4.42±0.09	1.87	4.08
4j	-4.25±0.08	1.98	5.16
(±)-5a	-3.67±0.07	1.14	3.79
(±)-5b	-3.92±0.05	2.01	5.55

[a] Log S (mol/L). Measured at pH 7.40 in 50 mM Tris-HCl, pH 7.4, at room temperature. Data are the mean ± SEM of three independent assays. [b] Extrapolated value at 65% of ammonium acetate buffer (pH 5.00) from six measurements. Mobile phase: methanol/ammonium acetate buffer (pH 5.00, 20 mM) v/v from 70% to 45%. Data are the mean ± SEM of three independent assays. [c] Bio-Loom version 1.6, Biobyte Corp., Claremont, U.S.A.

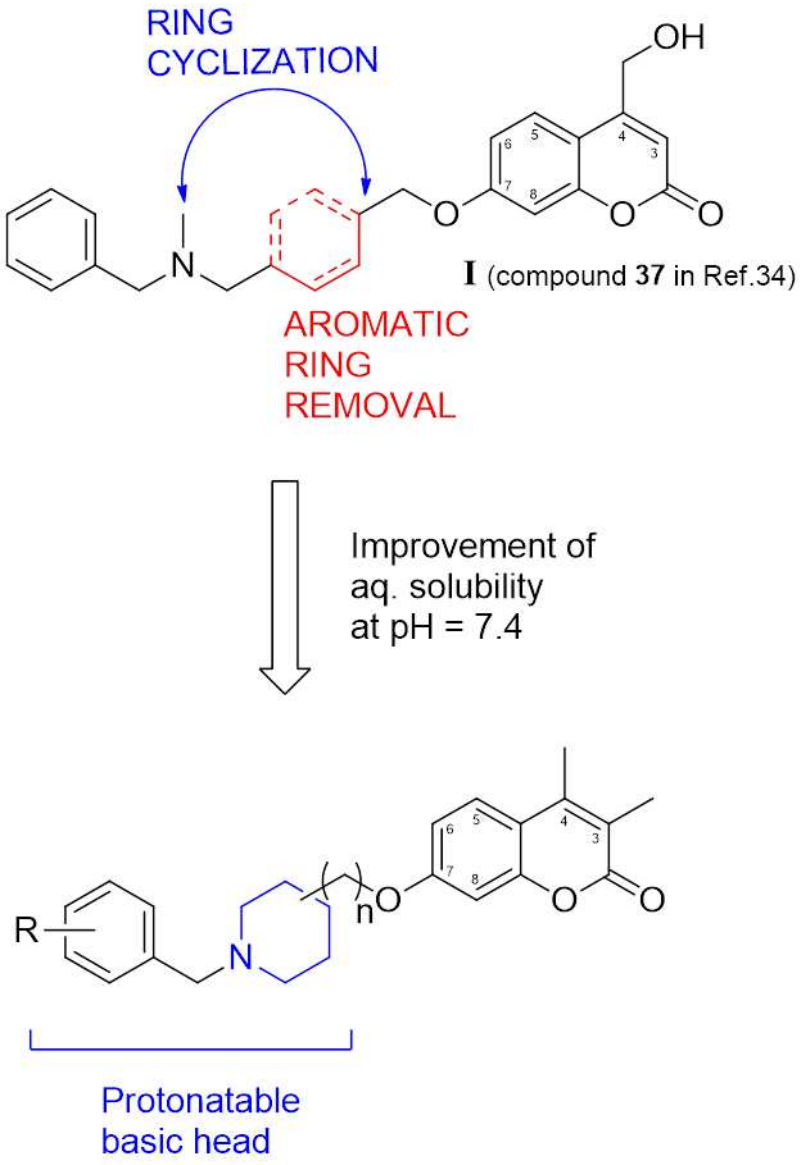

Figure 1. Rational Design

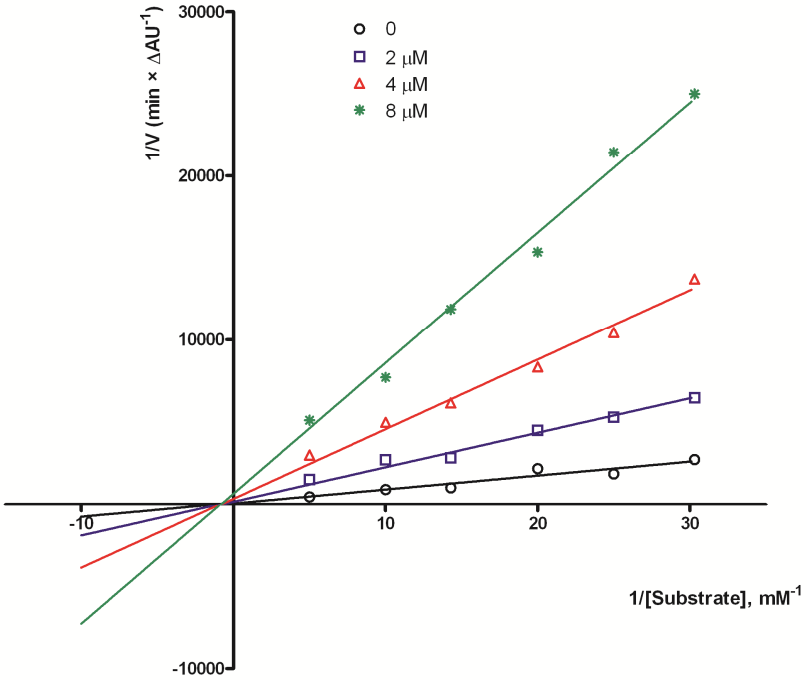

Figure 2. Lineweaver-Burk plots of *ee*ACHE inhibition kinetics of compound (±)-**5b**. Reciprocals of enzyme activity (eeAChE) *vs.* reciprocals of substrate (S-acetylthiocholine) concentration in the presence of different concentrations (0-8 μM) of inhibitor. Concentrations used for inhibitors are coded with different graphic symbols as reported in insets.

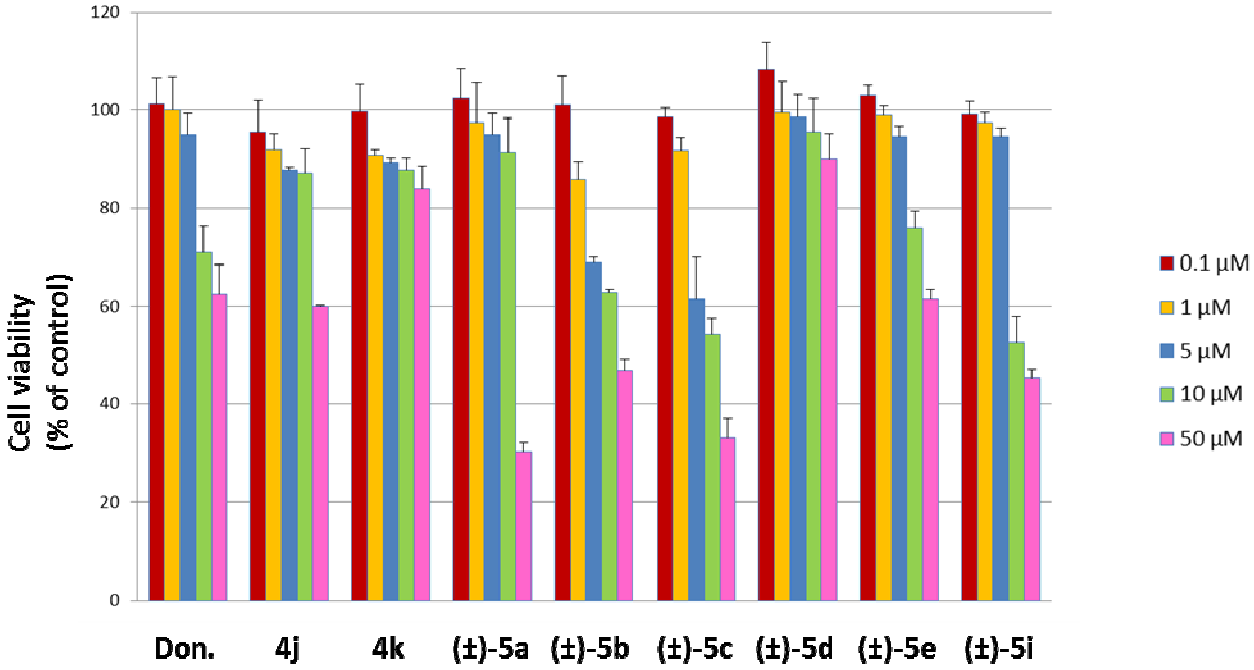

Figure 3. Cytotoxicity of compounds **4j-k**, (±)-**5a-e** and (±)-**5i** tested at concentrations in the range 0.1-50 µM in human neuroblastoma SH-SY5Y cell lines for 24 h. Data are reported as percentage of cell survival vs. untreated cells (control). Data represent means ± SD (n = 3).

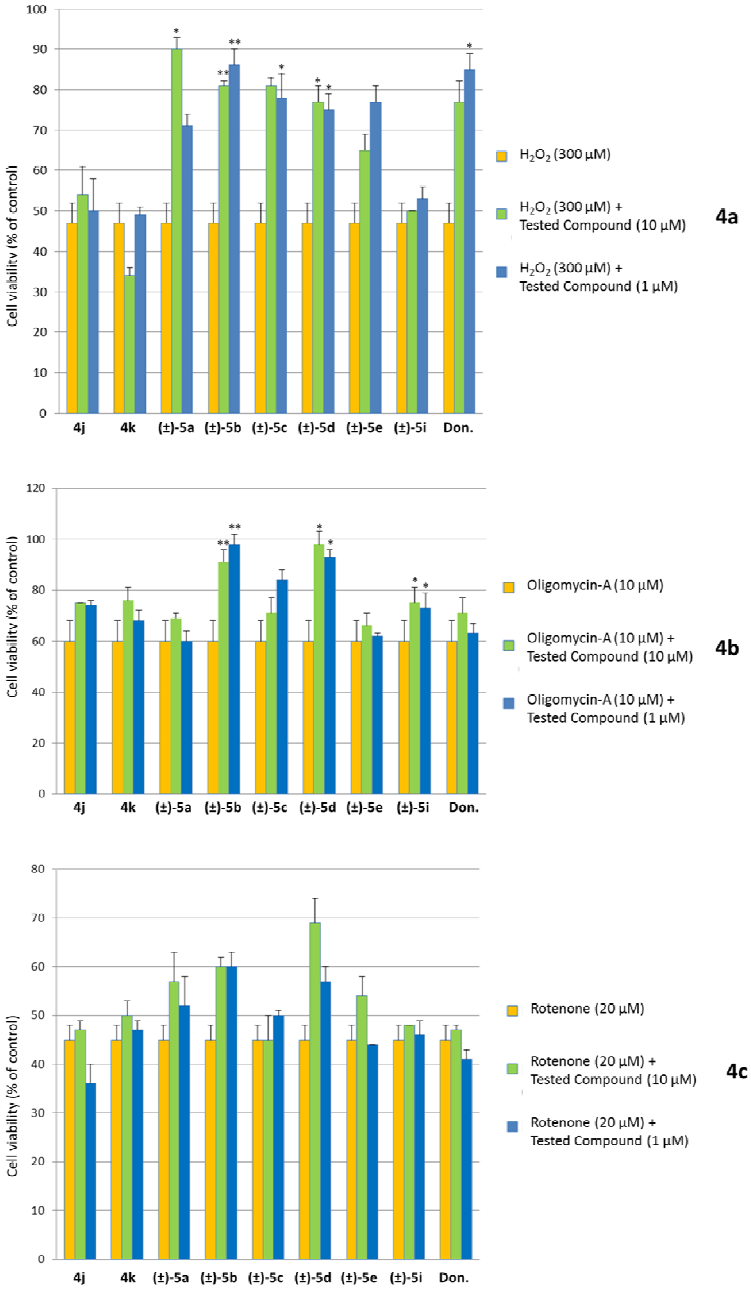

Figure 4. Neuroprotective effect on human neuroblastoma SH-SY5Y cells of selected compounds **4j-k**, (±)-**5a-e** and (±)-**5i** after 24 h incubation at different concentrations (1 and 10 µM) with H_2O_2 (300 µM, Figure 4a), oligomycin-A (10 µM, Figure 4b), and rotenone (20 µM, Figure 4c). Data are expressed as percentage of viable cells (referred to control) and shown as mean ± SD (n = 3). Untreated cells were used as control. Donepezil was used as a reference anti-AD marketed drug. Statistical significance was calculated using a two-way analysis of variance (ANOVA) followed by the Bonferroni post hoc tests (GraphPad Prism vers. 5); * $p < 0.05$, ** $p < 0.01$.

Table of Contents Graphic